the plant journal

The Plant Journal (2025) 121, e17267 doi: 10.1111/tpj.17267

# Rice RuBisCO activase promotes the dark-induced leaf senescence by enhancing the degradation of filamentation temperature-sensitive H

Yanli Zhang[1], Guojun Dong[2], Xiaoyue Wu[1], Fei Chen[1], Banpu Ruan[1], Yaohuang Jiang[1], Ying Zhang[1], Lu Liu[3], Yao-Wu Yuan[4], Limin Wu[1], Jian Wei[3,*], Qian Qian[2,*] and Yanchun Yu[1,3,*]

[1]College of Life and Environmental Sciences, Hangzhou Normal University, Hangzhou 310036, China,
[2]State Key Laboratory for Rice Biology, China National Rice Research Institute, Hangzhou 310006, Zhejiang, China,
[3]Faculty of Agronomy, Jilin Agricultural University, Changchun 130000, China, and
[4]Department of Ecology and Evolutionary Biology, University of Connecticut, Storrs, Connecticut 06269, USA

Received 3 April 2024; revised 21 December 2024; accepted 30 December 2024.
*For correspondence (e-mail weijian@jlau.edu.cn, qianqian188@hotmail.com and ycyu@hznu.edu.cn).

SUMMARY

Leaf senescence is a complex process that is triggered by many developmental and environmental factors. However, the mechanisms regulating leaf senescence remain unclear. Here, we revealed that rice ribulose-1,5-bisphosphate carboxylase/oxygenase activase (RCA) promotes the onset of basal dark-induced senescence. RCA was mainly expressed in the leaves, and its expression level quickly declined under dark conditions. Furthermore, rca mutant plants presented a prolonged leaf longevity phenotype in the dark, whereas overexpression of the large isoform of RCA ($RCA_L$), not small isoform ($RCA_S$), in rice and Arabidopsis accelerated leaf senescence. Filamentation temperature-sensitive H (OsFtsH1), a zinc metalloprotease, interacts with $RCA_L$ and $RCA_S$ and presents a higher binding efficiency to $RCA_L$ than $RCA_S$ in darkness. Furthermore, we found that $RCA_L$ promotes 26S proteasome-mediated degradation of OsFtsH1 protein, which can be inhibited by protease inhibitor MG132. Consequently, OsFtsH1 loss-of-function mutants exhibit accelerated leaf senescence, whereas OsFtsH1-overexpressing plants display delayed senescence. Collectively, our findings highlight the significant role of $RCA_L$ isoform in regulating leaf senescence under dark conditions, particularly through enhancing the degradation of OsFtsH1.

Keywords: rice (Oryza sativa L.), RuBisCO activase (RCA), dark-induced senescence (DIS), filamentation temperature-sensitive H (OsFtsH1), chloroplast.

## INTRODUCTION

Leaf senescence is a complex, highly coordinated, and probably orderly process that involves several physiological and molecular processes, such as the breakdown of proteins and chlorophyll, reallocation of nutrients, increase in reactive oxygen species (ROS), enhanced programmed cell death/necrosis, membrane ion leakage, and differential expression of many genes (Have et al., 2017; Sarwat et al., 2013; Woo et al., 2019). Plants undergo senescence due to abiotic factors, such as hormones, high salinity, prolonged darkness, nutrient deficiency, extreme temperatures, and drought, as well as biotic factors, such as ageing and pathogen attack (Guo & Gan, 2012; Sakuraba et al., 2018; Woo et al., 2019). Various internal or external cues can cause premature senescence, which severely reduces the post-harvest shelf life and results in a significant loss in agricultural yield. In contrast, efficient senescence maximizes viability in subsequent generations and seasons (Hortensteiner & Feller, 2002; Schippers et al., 2015; Zhang et al., 2022).

Dark-induced senescence (DIS) induces the expression of senescence-associated genes (SAGs) to initiate synchronized senescence in leaves (Fukao et al., 2012; Gao et al., 2012). Many functional SAGs have been identified using a dark-detached system, which has been widely used as an intracellular senescence model to investigate age-triggered senescence (Song et al., 2014). According to Li et al. (2020), SAGs include transcription factors, metabolic regulators, and receptors that convey hormones or signals related to stress responses (Li et al., 2020). The reduction of chlorophyll content is also considered to be a classic extracellular sign of leaf senescence, as chlorophyll is drastically reduced in plants under DIS conditions. In total, a substantial number of genes, including those belonging to families

of transcriptionally controlled transcription factors such as Tryptophan-Arginine-Lysine-Tyrosine (WRKY), basic helix-loop-helix (bHLH), NAM/ATAF1/2/CUC2 (NACs), ethylene response factor (ERF) and myelocytomatosis/myeloblastosis (MYC/MYBs), altered their expression under DIS and contributed to leaf senescence, according to a transcriptome analysis of rice leaves exposed to darkness (Lakshmanan et al., 2015). A senescence phenotype that is accelerated by darkness is observed in transgenic plants that overexpress OsEIL2, a rice transcription factor that mimics ethylene-insensitive 3, but OsEIL2-RNAi plants exhibit the opposite phenotype (Jin et al., 2020). OsWRKY5 promotes leaf senescence under both naturally occurring and DIS conditions by upregulating the expression of senescence-induced NAC, abscisic acid (ABA) biosynthesis, and chlorophyll degradation genes (Kim et al., 2019). Additionally, senescence is linked to the upregulation of the SAGs OsS40-1, OsS40-7, OsS40-12, OsS40-13, and OsS40-14, which are upregulated in response to dark treatment (Habiba et al., 2021). Green leaves were retained significantly longer by OsMYB102-overexpressing transgenic lines than by the wild type under ABA-induced, dark-induced, and natural senescence conditions. Furthermore, under both dark-induced and ABA-induced leaf senescence conditions, an osmyb102 knockout mutant displayed accelerated senescence phenotype, suggesting that OsMYB102 plays a major role in the process of leaf senescence (Piao et al., 2019). In addition to ABA, other plant hormones involved in the control of DIS include jasmonic acid (JA), salicylic acid (SA), and ethylene (Jan et al., 2019; Jibran et al., 2013). Under DIS conditions, a rice jasmonate ZIM-domain protein (OsJAZ8) negatively controls JA-mediated leaf senescence (Uji et al., 2017). In contrast, osmed25 mutants delayed JA-regulated leaf senescence under DIS (Suzuki et al., 2021). The submergence tolerance regulator SUBMERGENCE1A (SUB1A) can alter the response to extended darkness by limiting ethylene synthesis and the response to JA and SA. Consequently, this may lessen the accumulation of messenger RNAs associated with senescence and the breakdown of carbohydrates and chlorophyll (Fukao et al., 2012).

In green plants, ribulose-1,5-bisphosphate carboxylase/oxygenase (RuBisCO) catalyzes the irreversible carboxylation of ribulose-1,5-bisphosphate and $CO_2$ to generate two 3-phosphoglyceric acid molecules (Flecken et al., 2020; Miziorko & Lorimer, 1983). A member of the huge $AAA^+$ superfamily proteins, RuBisCO activase (RCA), can modify the structure of RuBisCO, activate it in vivo, and remove inhibitory sugar phosphates and carbamylation from its catalytic sites (Bracher et al., 2017; Jin et al., 2006). In the past few decades, several researchers have discovered that RCA serves as a multifunctional stress responder in addition to its activation feature on RuBisCO (Chen et al., 2015; Waheeda et al., 2023). Transgenic rice plants that co-overproduce RCA and RuBisCO enhance photosynthesis in the ideal temperature range of 32–40°C. Nonetheless, at 25°C, the rates of $CO_2$ assimilation matched those of wild-type plants (Qu et al., 2021; Suganami et al., 2021). The RCA isoforms found in rice, known as large ($RCA_L$) and small ($RCA_S$), are produced by the alternative splicing of RCA from a single nuclear gene (Nagarajan & Gill, 2018; To et al., 1999; Werneke et al., 1989; Zhang & Komatsu, 2000). According to Wang et al. (2010), heat stress dramatically increased the expression of $RCA_L$ but had little effect on the expression of RCAs (Wang et al., 2010). Thus, transgenic rice plants expressing increased amounts of $RCA_L$ exhibit higher thermotolerance and grow better at high temperatures than wild-type and transgenic rice plants expressing RCAs (Wang et al., 2010). Moreover, it has been suggested that N supply affects RuBisCO content when RCA is overexpressed. Additionally, 10–20% less RuBisCO was found in RCA-overproducing plants at 0.5 mM-N (0.25 mM $NH_4NO_3$) and 2.0 mM-N (1.0 mM $NH_4NO_3$) supplements in nutrient solution. Conversely, at 8.0 mM-N (2.5 mM $NH_4NO_3$ plus 3.0 mM $NaNO_3$), RuBisCO content remained unchanged (Suganami et al., 2018, 2020). However, studies have shown that under variable light conditions, RCA-induced activation of RuBisCO can hinder photosynthesis (Salvucci et al., 1986; Zhang et al., 2002). Transgenic rice plants overproducing RCA had a higher activation state of RuBisCO and faster induction of photosynthesis when exposed to high light intensities (Zhang et al., 2002). Additionally, an "$H_2O_2$ burst" in the chloroplast was brought on by infection with Oryza meyeriana and Xanthomonas oryzae pv. oryzae (Xoo), leading to the redistribution of RCA from the chloroplast stroma to the thylakoid membrane (Yang et al., 2011). This redistribution of RCA to the thylakoid membrane under light conditions protects the membrane from $H_2O_2$-induced oxidative damage (Mei et al., 2019). Furthermore, proteomic research has identified rice protein patches, including RCA isoforms, that are significantly altered in response to drought (Ji et al., 2012; Salekdeh et al., 2002). $RCA_L$-overexpressing plants were more vulnerable to drought stress than the wild type, whereas $RCA_S$-overexpressing plants showed a mildly drought-sensitive phenotype (Fan et al., 2022). Fan et al. found that Ghd2 significantly accelerated leaf senescence and enhanced $RCA_L$ expression in drought-affected plants (Fan et al., 2022).

In the present investigation, we identified a rice RCA, especially the large isoform $RCA_L$, which interacts with chloroplast-localized filamentation temperature-sensitive H (OsFtsH1) and accelerates the degradation of OsFtsH1. Dark stress downregulates the expression level of RCA and promotes the degradation of RCA protein, resulting in the stabilization and accumulation of OsFtsH1 protein, which helps plants cope with prolonged dark stress. Taken together, our results demonstrate that RCA is an activator of RuBisCO and a repressor of OsFtsH1 to affect DIS.

## RESULTS

### RCA is a member of dark-suppressed protein in rice

When only a portion of the plant is affected, light deprivation, in the form of intense shade or darkening of leaves, causes rapid senescence in many plant species (Keech et al., 2010; Liebsch & Keech, 2016). Therefore, transcriptome sequencing of rice samples exposed to darkness allowed us to better understand the mechanisms underlying shade-induced senescence and DIS. To conduct the DIS transcriptomic analysis, RNA samples were taken from rice plants exposed to darkness at different times. After dark treatment for 4 h, 1348 upregulated genes and 1481 downregulated genes were identified, as shown in the volcano plot ($P \leq 1e\text{-}10$ for both upregulated and downregulated genes) (Figure S1A; Table S1). These genes were concentrated in more than 10 pathways obtained by KEGG pathway enrichment analysis (Figure S1B). Among the differentially expressed genes (DEGs) involved in photosynthesis, most were involved in photosystem I, photosystem II (PSII), and chlorophyll degradation (Figure S1C–E). RCA, a presumed photosynthetic activator, showed a declining expression pattern during DIS (Figure S1C). Similar results have been obtained using microarray analysis in Arabidopsis (Song et al., 2014; van der Graaff et al., 2006). Thus, RCA was selected, and its potential role in the DIS was investigated. Quantitative reverse transcription-polymerase chain reaction (qRT-PCR) revealed that the expression of both $RCA_L$ and $RCA_S$ rapidly decreased in response to 3 h of dark treatment and was retained at only 5% after 12 h of dark treatment (Figure 1A). Using an antibody specifically recognizing the RCA C-terminal (Figure S2), immunoblot analysis revealed that the amount of both $RCA_L$ and $RCA_S$ proteins was gradually reduced by dark treatment and the decline was not affected by the application of 26S protease inhibitor MG132 (Figure 1B), indicating that the degradation of RCA during dark treatment is independent of proteasome degradation pathway. In both MG132-treated and untreated samples, RCA expression levels remained low after 2 and 6 days of dark treatment (Figure 1C). Similarly, RCA protein significantly decreased in the area of the blade where natural senescence began (Figure 1D). Thus, both the transcriptional and protein levels of RCA might be involved in leaf senescence caused by ageing and darkness, and the transcriptional regulation of RCA may play a major role.

According to protein domain analysis by Conserved Domain Search (CD-SEARCH) via the National Center for Biotechnology Information (NCBI) website, RCA has a conserved domain with some ATP-binding sites (amino acid positions 154–298) of the $AAA^+$ protein family (Figures S3A and S4), which frequently perform chaperone-like functions that aid in the assembly, operation, or disassembly of protein complexes (Neuwald et al., 1999; Olivares et al., 2016). Phylogenetic analysis was conducted using the protein sequences of the rice RCA protein and its homologous proteins from other species. The results showed that the rice RCA protein exhibited very high sequence homology with other RCA proteins from gramineous plants, such as Hordeum vulgare, Triticum aestivum, Phragmites australis, Sorghum bicolor, and Zea mays, forming a distinct clade (marked blue) and separating from clades of eudicots (marked red) and algal (marked green) plants (Figure S3B). Representative species of green plants exhibit conserved sequence similarities in RCA proteins, as demonstrated by amino acid alignment and LOGO analysis of the protein domains. Interestingly, monocot and eudicot plants show greater similarity to each other than to the green alga Auxenochlorella pyrenoidosa, with five fully conserved amino acid differences in the studied plants and seven differences in fairly conserved amino acids between the groups (Figure S3C). This observation suggests that although RCA proteins are conserved within monocots and eudicots, the distinct differences imply that A. pyrenoidosa has followed a unique evolutionary path that diverges from that of terrestrial species.

### Expression pattern and subcellular localization

Rice has long been recognized to have two isoforms of RCA; however, little is known about the expression patterns of $RCA_L$ and $RCA_S$ in different rice tissues (Zhang & Komatsu, 2000). In this study, qRT-PCR and semi-quantitative RT-PCR were used to examine the expression of $RCA_L$ and $RCA_S$ in various tissues. As shown in Figure 1, $RCA_S$ was mainly expressed in green tissues, with the highest expression level in leaves, followed by the stem and leaf sheath, whereas it was weakly expressed in roots and panicles (Figure 1E). Additionally, the expression level of $RCA_L$ was noticeably lower than that of $RCA_S$ in all tissues. Semi-quantitative RT-PCR performed on the same tissues verified these expression patterns (Figure 1F). Immunoblot analysis of total protein extracts from various wild-type plant tissues was performed to further ascertain RCA expression in these tissues. Consistent with the qRT-PCR results, immunoblot analysis indicated that both $RCA_L$ and $RCA_S$ proteins accumulated primarily in the leaves (Figure 1G).

Next, we performed subcellular location analysis of $RCA_L$-green fluorescence protein (GFP) and $RCA_S$-GFP in rice cells after identifying the RCA expression pattern. Using PEG-mediated protoplast transient transformation, 35S::GFP, 35S::$RCA_L$-GFP, and 35S::$RCA_S$-GFP were introduced into the rice protoplasts. As shown in Figure 1(H–J), the fluorescence signal distributions of $RCA_L$-GFP and $RCA_S$-GFP co-localized with chloroplast spontaneous fluorescence, whereas the fluorescence of the free GFP was dispersed throughout the cytoplasm. These findings suggest that RCA is primarily localized in chloroplasts.

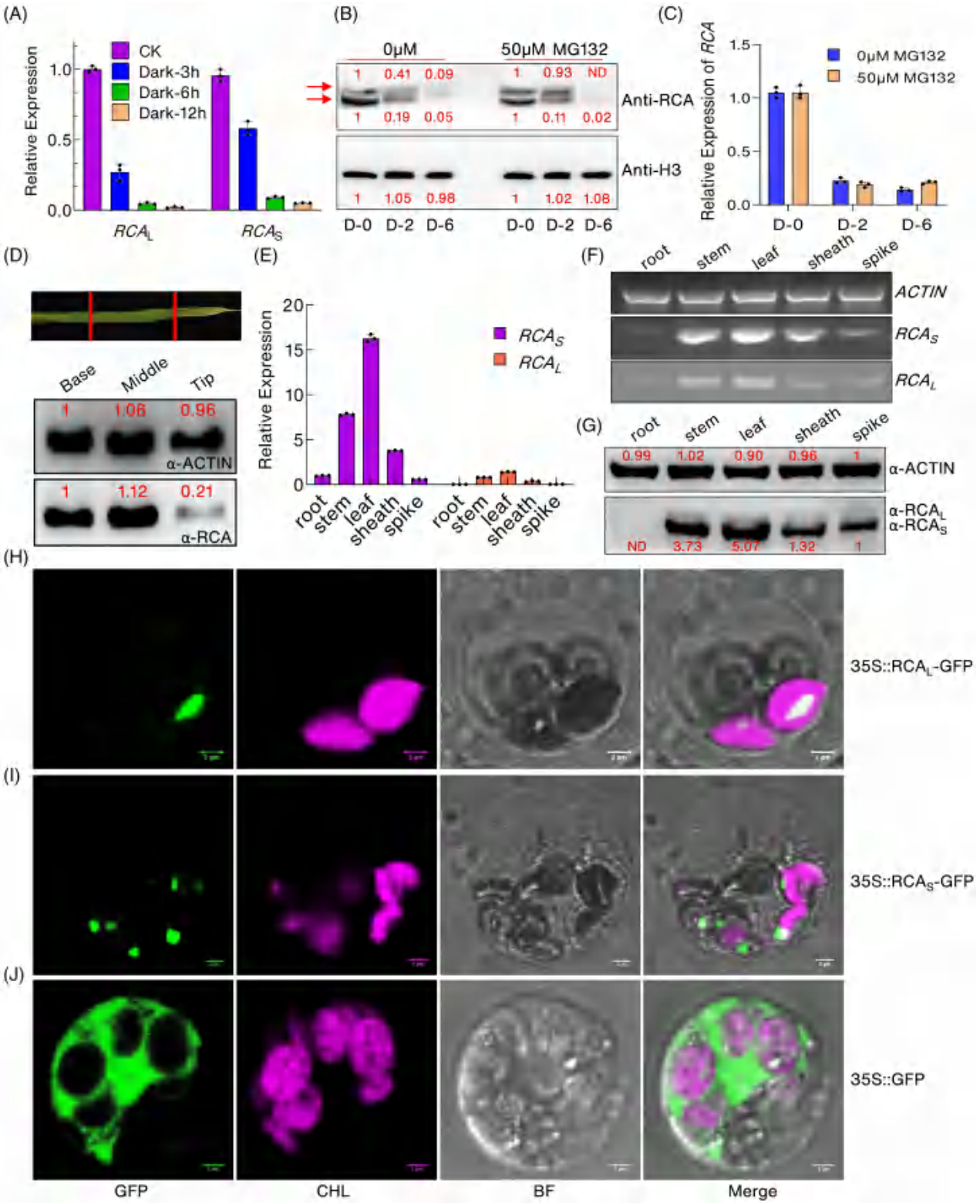

Figure 1. RCA is a dark-suppressed protein in chloroplast.
(A) Expression of $RCA_S$ and $RCA_L$ in response to dark treatment. Two-week-old wild-type plants were treated, and leaves were pooled for RNA extraction. Expression was determined by qRT-PCR. The CK samples were set as "1." This experiment has been repeated three times.
(B) Immunoblot analysis using anti-RCA antibody to show RCA protein levels with and without MG132 treatment after dark treatment for different times. To block proteasomal protein degradation, rice seedlings were pre-treated with 50 lM MG132 for 2 h and then treated with darkness. D-0, dark treatment for 0 day; D-2, dark treatment for 2 days; and D-6, dark treatment for 6 days. Western blot against histone H3 served as loading control. Quantifications (red numbers) were obtained from Image Lab software. ND, not detected.
(C) Expression levels of RCA with and without MG132 treatment after dark treatment. Histone H3 was used as the control. The expression levels on D-0 were set as "1." D-0, dark treatment for 0 day; D-2, dark treatment for 2 days; and D-6, dark treatment for 6 days. This experiment has been repeated three times. Data are means of three replicates with SD.
(D) Western blotting experiment detected the protein levels of RCA in a senescing leaf. One-month-old leaves showing approximately 20% senescence were dissected into three parts as indicated. Western blot against actin served as loading control. Quantifications (red numbers) were obtained from Image Lab software.
(E) Expression of $RCA_L$ and $RCA_S$ in various organs analyzed by qRT-PCR analysis. All the materials were harvested from a mature wild-type plant. Actin was used as the internal control.
(F) Expression of $RCA_L$ and $RCA_S$ in various organs analyzed by semi-quantitative PCR analysis. Actin was used as the internal control.
(G) Immunoblot analysis of RCA in various organs in the wild-type plant. Western blot against actin served as loading control. Quantifications (red numbers) were obtained from Image Lab software. ND, not detected.
(H) Subcellular localization of 35S::$RCA_L$-GFP.
(I) Subcellular localization of 35S::$RCA_S$-GFP.
(J) The binary vector containing 35S::GFP was transiently expressed in rice protoplasts. GFP, green fluorescence protein. BF, bright field; CHL, chlorophyll fluorescence. Scale bars = 2 lm.

## Knockdown of RCA causes delayed dark-induced leaf senescence

To determine the function of RCA in vivo, the T-DNA insertion mutant line PFG_1B-13 514 (hereafter designated as rca; wild type is Dongjin, hereafter designated as DJ) was isolated from a T-DNA insertion mutant library (Jeon et al., 2000; Jeong et al., 2006). The T-DNA was inserted into the 5′ untranslated region (−285) of the RCA gene (Figure S5A), reducing RCA expression in homozygous rca plants to 30% of that in wild-type plants, as determined by qRT-PCR and semi-quantitative RT-PCR (Figure S5B–D). Additionally, immunoblot analysis revealed that the rca mutant had lower levels of both $RCA_S$ and $RCA_L$ proteins compared with the wild-type plant (Figure S5E), indicating that rca is a knockdown mutant. In addition, the rca mutant had lower chlorophyll content in leaves than wild-type plants during the first week of growth and exhibited a pale-green phenotype in 5-day-old and 7-day-old seedlings when they were planted in both the greenhouse and field (Figure S6A–D). However, when the seedlings grew to 10 days of age, the phenotype of pale-green leaves of rca gradually recovered, and there was no variation identified in the determination of pigments (Figure S6E,F).

To determine whether RCA is associated with DIS, leaf segments of wild-type (DJ) and rca plants were incubated in 3 mM MES buffer at 27°C in the dark. After 8 days of dark treatment, wild-type leaves completely turned yellow, whereas rca leaves still had some green pigment remnants (Figure 2A). To eliminate variations in the developmental stage, we assessed the expression levels of senescence genes SGR and NAP in DJ and rca mutants and found no significant differences in their expression during the seedling stage (Figure S7A,B). We further compared the tolerance of mutant seedling leaves at the 21-day-old stage with wild-type leaves at various developmental stages (15 and 21 days) under dark treatment for 8 days. The results showed that compared to wild-type seedlings with the same growth period or those that were 6 days younger, leaf segments of the rca mutant both exhibited a delayed senescence phenotype (Figure S7C,D). Meanwhile, $H_2O_2$ content also increased significantly in the wild type compared with the rca mutant (Figure 2B). As a biomarker of photosynthetic efficiency and stability of PSII in response to stress, the Fv/Fm (the ratio of variable (Fv) to maximum (Fm) fluorescence) of rca and wild-type plants was measured using chlorophyll fluorescence imaging (Figure 2C–E). On the 4th, 6th, and 8th days of dark treatment, the Fv/Fm ratio in the rca mutant was significantly higher than those in the wild type (Figure 2D,E), and the final chlorophyll content was also higher (Figure 2F). Next, we examined the phenotype of the rca mutant during DIS in the whole plant. Following 10 days of dark incubation, the majority of rca leaves remained green, but many wild-type leaves became yellow, which resembled the leaf segment assay (Figure 2G,H). To further verify the conservation of RCA function in DIS, we produced rca-ami plants in different wild-type backgrounds (Nipponbare, short for NIP) using artificial miRNAs (amiRNAs) method and examined whether the rca-ami allele exhibited a delayed senescence phenotype similar to that of rca plants (Figure S8A). The rca-ami mutant we generated was a severe knockdown allele because only a few RCA transcripts and proteins remained in the mutant leaves (Figure S8B,C). During DIS, the leaf segments of rca-ami also displayed a delayed senescence phenotype (Figure S8D). These findings suggest that RCA may act as an activator of leaf senescence in the DIS assay.

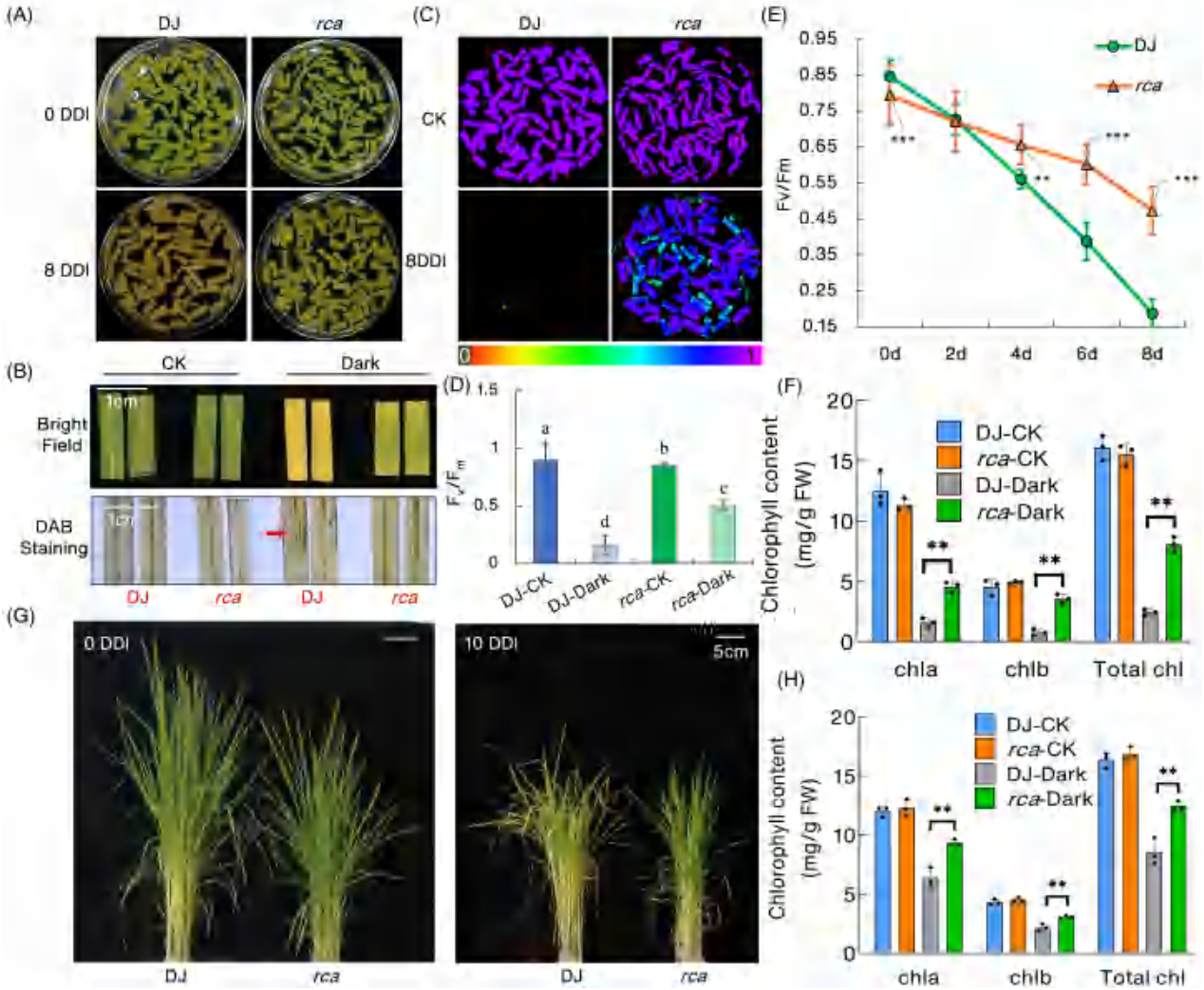


Figure 2. rca mutant displayed delayed dark-induced leaf senescence.
(A) The color change that occurs in leaf segments of DJ (wild type, Dongjin) and rca during DIS. They were incubated in 3 mM MES (pH 5.8) buffer with the abaxial side up at 27°C in darkness.
(B) Leaves incubated in dark for 8 days were stained with DAB. Scale bar = 1 cm.
(C) Fv/Fm images obtained from chlorophyll fluorescence using the PlantView230F imaging system before and after dark treatment.
(D) Fv/Fm values. Data are means of three replicates with SD. Different letters indicate significant differences between DJ and rca plants with or without dark stress (8 days for dark), according to one-way ANOVA and Tukey's multiple-range tests ($P < 0.05$).
(E) The Fv/Fm values of DJ and rca plants under normal conditions and dark treatment at different time points. Values are presented as means ± SD, and the statistically significant differences were determined by Student's t-test (biological replicates, n = 4, **$P < 0.01$, ***$P < 0.001$).
(F) Chlorophyll content of leaves in (A).
(G) DJ and rca whole plants were grown for 1 month under LD (14-h light/day) conditions and then were transferred to darkness at 28°C for 10 days (10 DDI). Scale bars = 5 cm.
(H) Chlorophyll content of leaves in (F). Mean and SD values in (F, H) were obtained from at least three biological replicates. Asterisks indicate significant difference (Student's t-test, **$P < 0.01$). DDI, day(s) of dark incubation.

## $RCA_L$ overexpression promotes DIS both in rice and Arabidopsis

To determine the roles of $RCA_L$ and $RCA_S$ in influencing leaf senescence, we generated both $RCA_L$- and $RCA_S$-overexpressing lines in the NIP background by introducing each CDS sequence, followed by GFP and His tags (HisT for short), into pCAMBIA2300 vector driven by ubiquitin promotor (Figure S9A). According to qRT-PCR and semi-quantitative RT-PCR analysis, the expression levels of either $RCA_L$ or $RCA_S$ were hundreds of times higher than those in the wild type (Figure S9B–D,F–H). Additionally, employing the GFP tag, HisT, and its particular antibody, immunoblot analysis revealed that both $RCA_S$ and $RCA_L$ proteins were largely accumulated in transgenic plants (Figure S9E,I).

Next, for phenotypic characterization under dark conditions, we used two representative lines of each T2 transgenic rice seedling ($RCA_L$-OE-1, $RCA_L$-OE-2, $RCA_S$-OE-1, and $RCA_S$-OE-2) (Figure S9B–I). Transgenic and wild-type plants did not show significant differences under typical growth conditions, and there was no difference in the expression levels of senescence genes during the seedling stage (Figure S10). Six days after dark treatment, both $RCA_L$- and $RCA_S$-overexpressing lines, particularly $RCA_L$-overexpressing lines, showed severe yellowing of leaves (Figure 3A,B). There was a noticeable difference in the amount of chlorophyll between the wild-type and RCA-overexpressing lines after dark treatment (Figure 3C,D). Additionally, after the plants were exposed to dark treatment for 6 days, leaves from $RCA_L$- and $RCA_S$-overexpressing plants showed more intense staining with DAB than leaves from wild-type plants, suggesting a greater build-up of $H_2O_2$ (Figure 3E). Consistently, dark treatment using detached leaf segments resulted in the same earlier senescence phenotype in overexpression lines (Figure 3F). To assess whether RCA overexpression affects the integrity of the photosynthetic machinery, we analyzed the relative change in Fv/Fm values after dark treatment. The values of Fv/Fm in $RCA_L$-OEs were markedly lower and declined faster than those in the wild-

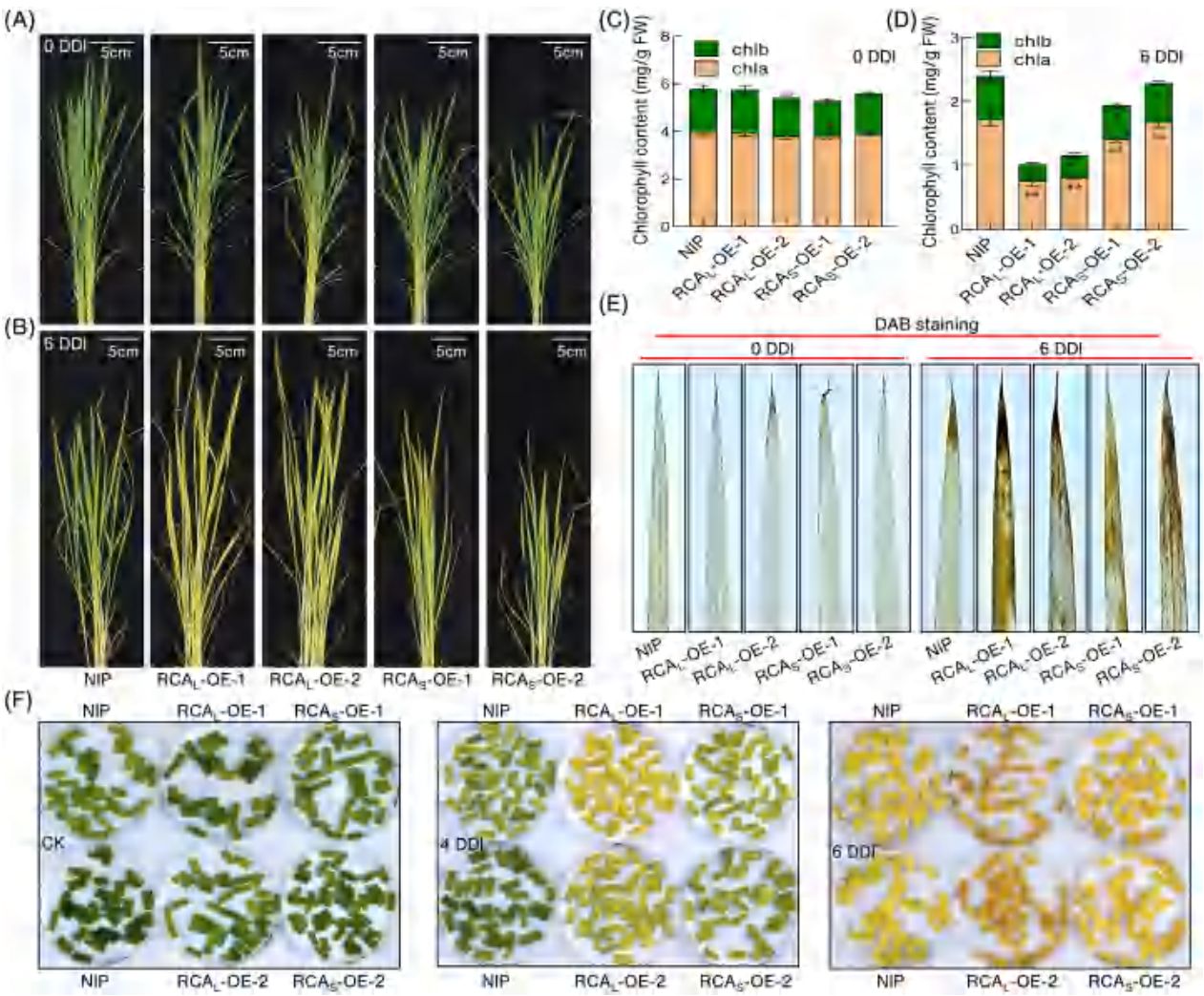


Figure 3. RCA reduces tolerance to prolonged darkness.
(A) Phenotype of NIP, $RCA_L$-OE-1, $RCA_L$-OE-2, $RCA_S$-OE-1, and $RCA_S$-OE-2 plants under regular growth conditions. Scale bar = 5 cm.
(B) Phenotype of NIP, $RCA_L$-OE-1, $RCA_L$-OE-2, $RCA_S$-OE-1, and $RCA_S$-OE-2 plants with 6 days of complete darkness. Scale bar = 5 cm.
(C) Chlorophyll content of NIP, $RCA_L$-OE-1, $RCA_L$-OE-2, $RCA_S$-OE-1, and $RCA_S$-OE-2 plants in (A).
(D) Chlorophyll content of NIP, $RCA_L$-OE-1, $RCA_L$-OE-2, $RCA_S$-OE-1, and $RCA_S$-OE-2 plants in (B). Values are presented as means ± SD, and the statistically significant differences were determined by Student's t-test (biological replicates, n = 20, *P < 0.05, **P < 0.01).
(E) DAB staining of leaves with and without dark treatment for 6 days.
(F) Leaves of NIP, $RCA_L$-OE, and $RCA_S$-OE were treated with darkness for 4 and 6 days and photographed.

type plant after dark treatment, while the values of Fv/Fm in $RCA_S$-OEs were slightly lower than those in the wild type (Figure S11). Since lower Fv/Fm values are often observed in mutants defective in PSI, PSII, or the cytochrome b6f complex (Kato et al., 2018), we inferred that $RCA_L$-OEs might be defective in photosynthetic protein complexes.

To investigate whether RCA function in dark-induced leaf senescence is conserved between rice and Arabidopsis, we isolated a homozygous Atrca T-DNA insertion line (SALK_003204). Sequence analyses showed that double T-DNAs were inserted in the 5′ untranslated region, 223 base pairs upstream of the start codon (Figure S12A,B). Similar to the rice rca mutant, the Atrca mutant retained 20% of its expression level compared with wild-type Col and had pale-yellow leaves at the seedling stage (Figure S12C–G). We then transformed rice $RCA_S$ and $RCA_L$ into Atrca plants, and the transcription and translation levels of $RCA_S$ and $RCA_L$ were analyzed in two representative homozygous T3 transgenic lines (Figure S13A–E). We found that the Atrca phenotypes, such as pale-yellow and shorter leaves, were fully restored in transgenic plants (Figure S14A). Moreover, after 8 days of dark treatment, $RCA_L$-OEs lines exhibited a more severe senescence phenotype compared with Col. In contrast, the Atrca mutant had more green leaves than the Col plants (Figure S14B). Consistent with the visible yellow leaf phenotype, the chlorophyll content of $RCA_L$-overexpressing lines was lower than that of Col (Figure S14C,D). Collectively, the RCA exhibits its consistent role in monocotyledonous rice and dicotyledonous Arabidopsis, as the presence of $RCA_L$ in rice and Arabidopsis both accelerate the process of dark-induced leaf senescence.

## $RCA_L$ interacts with OsFtsH1 in the chloroplast

To further investigate how RCA affects dark-induced leaf senescence, we investigated the interacting partners of RCA by immunoprecipitation using $RCA_L$-OE plants. Co-immunoprecipitation (Co-IP) against a monoclonal anti-HisT antibody was performed using purified total proteins from various plants. Five distinct bands were detected by sodium dodecyl sulfate (SDS)-PAGE and staining of the $RCA_L$-OE plant. No band was observed at the same location in the control lane. The probable proteins that interact with $RCA_L$ were then identified by LC–MS/MS analysis of the Co-IPed proteins (Figure S15A,B). Subsequently, LC–MS/MS data revealed that one of the candidate proteins that piqued our curiosity was the ATP-dependent zinc metalloprotease (OsFtsH1) (Figure S15C), homologous proteins of which have been reported to be involved in the degradation of the D1 protein (Kato et al., 2023; Krynicka et al., 2023; Liu et al., 2024). We used various techniques to investigate the physical interactions between $RCA_L$ and OsFtsH1. First, Y2H experiments revealed that $RCA_L$ and OsFtsH1 interacted in vitro (Figure 4A). We then performed bimolecular fluorescence complementation (BiFC), Co-IP, and colocalization assays to detect their interactions in vivo. Yellow fluorescent protein signals were detected in the chloroplasts of Nicotiana benthamiana leaf mesophyll cells by BiFC studies (Figure 4B), indicating that $RCA_L$ and OsFtsH1 in living tobacco cells interact directly. Moreover, $RCA_L$ co-precipitated with OsFtsH1-GFP, but not with GFP, when tagged proteins were transiently expressed in N. benthamiana leaves, further confirming the interaction between OsFtsH1 and $RCA_L$ (Figure 4C). Additionally, in the colocalization assay, GFP fluorescence contributed by $RCA_L$-GFP overlapped with OsFtsH1-mCherry fluorescence in the chloroplast (Figure 4D). Taken together, these in vitro and in vivo data indicate that $RCA_L$ and OsFtsH1 interact in chloroplasts.

Given that $RCA_S$ also plays its role in the context of dark-induced leaf senescence, even though its effect is less pronounced than $RCA_L$ (Figure 3), we investigated whether $RCA_S$ and OsFtsH1 interact as well. Likewise, the interaction between $RCA_S$ and OsFtsH1 was validated by Y2H assay (Figure 5A), Co-IP analysis (Figure 5B), and luciferase complementation imaging (LCI) assay (Figure 5C). Our Co-IP experiments showed that, under normal conditions, the OsFtsH1 protein appeared in both $RCA_L$ and $RCA_S$ patches with comparable efficiency (0.93:1) (Figure 5D), indicating that $RCA_L$ and $RCA_S$ could bind with OsFtsH1. However, under dark conditions, the abundance of OsFtsH1 in the $RCA_S$ patch was significantly reduced (statistical analysis: 1:7.63 compared with $RCA_L$-OE) (Figure 5E). These results indicate that OsFtsH1 prefers to interact with $RCA_L$ rather than $RCA_S$ in dark environments.

## $RCA_L$ promotes the degradation of OsFtsH1 protein

In order to investigate the biological significance of the RCA-OsFtsH1 physical interaction, we first measured the expression level and protein abundance of OsFtsH1 in both rca mutants and RCA-overexpressing plants at various intervals during dark treatment. qRT-PCR showed that the expression of OsFtsH1 was slightly higher in the rca mutant than in the wild-type plant and lower in the $RCA_L$-OE-1 plant from D-0 of dark processing to D-4. However, the change in OsFtsH1 expression in $RCA_S$-OE-1 plant was similar to wild-type plant (Figure 6A,B). Immunoblot analysis showed that in wild-type plants NIP and DJ, the level of OsFtsH1 protein accumulated significantly after 2 days of dark treatment, followed by a slight decline after 6 days (Figure 6C). Similarly, this trend was also observed in both $RCA_L$- and $RCA_S$-overexpressing plants. However, we found that the overall levels of OsFtsH1 protein in the RCA-overexpressing lines, particularly in $RCA_L$-overexpressing plants, were much lower than that in wild-type plants even under normal conditions (Figure 6C). In contrast, the OsFtsH1 protein abundance in

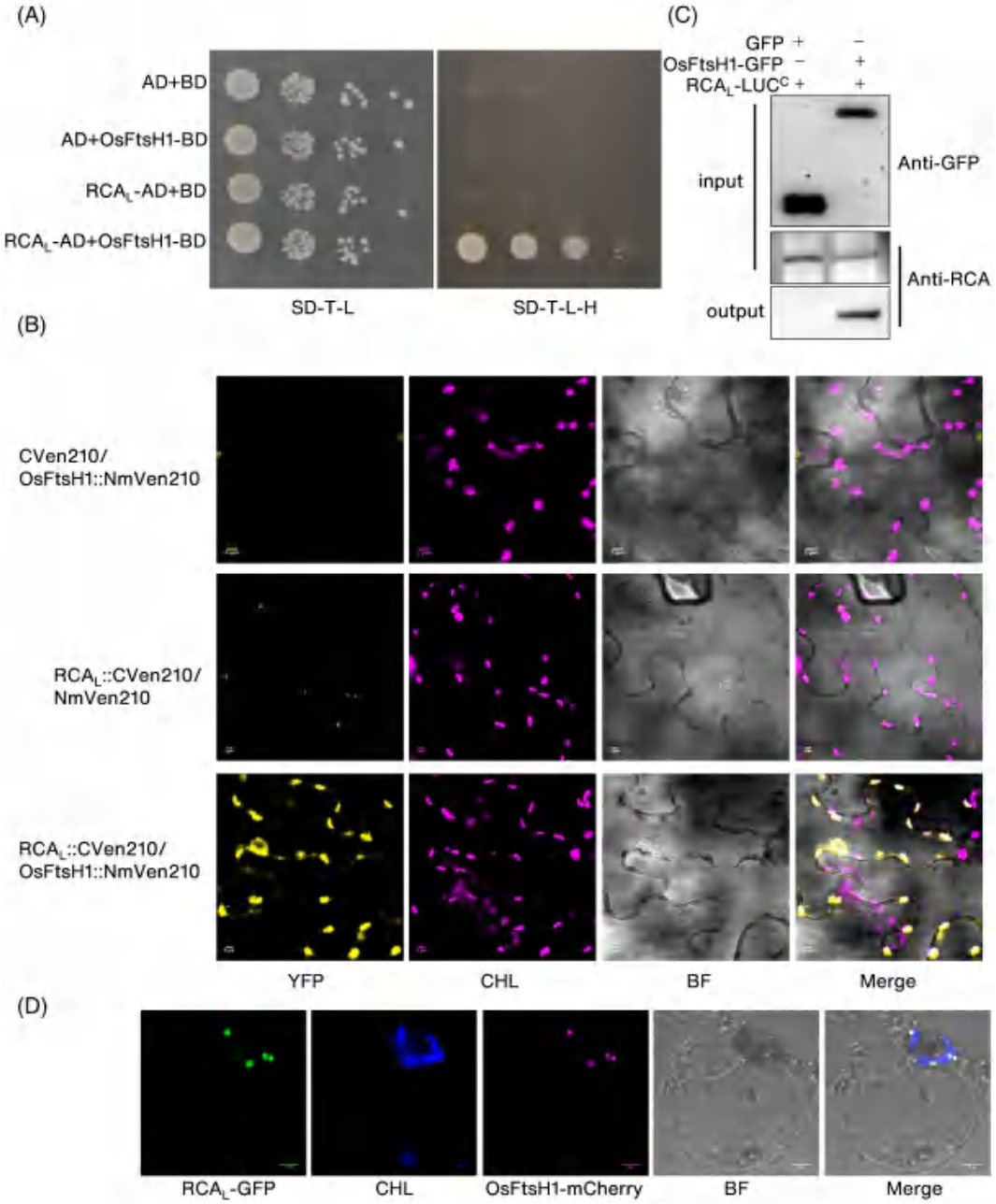


Figure 4. OsFtsH1 is the interacting protein of RCA$_L$.
(A) Y2H showed that OsFtsH1 interacts with RCA$_L$. SD-T-L, SD medium without Leu and Trp; SD-T-L-H, SD medium without Trp, Leu, and His. pGBKT7 + pGADT7, pGBKT7-OsFtsH1+ pGADT7, and pGBKT7 + pGADT7-RCA$_L$ were used as negative controls.
(B) BiFC analysis of in vivo interactions by transient expression in Nicotiana benthamiana. First column, OsFtsH1::NmVen210/CVen210 parent vector, shows little weak background signal; middle column, NmVen210/RCA$_L$::CVen210 parent vector shows little weak background signal; bottom column, OsFtsH1::NmVen210 interacts with RCA$_L$::CVen210. YFP (Yellow fluorescent protein) = mVenus BiFC; CHL, chlorophyll autofluorescence; BF, bright field.
(C) In vivo interaction between OsFtsH1-GFP and RCA$_L$ revealed by the co-immunoprecipitation assay. After immunoprecipitation with anti-GFP magnetic beads, precipitated proteins were probed with an anti-RCA antibody.
(D) RCA$_L$-GFP and OsFtsH1-mCherry fusion constructs were transiently expressed in rice protoplasts for subcellular localization analysis. BF, bright field; CHL, chlorophyll fluorescence. Scale bars = 4 lm.

the rca mutant was higher than that in the wild-type plant and maintained a consistently elevated level during dark treatment (Figure 6C, right panel). Meanwhile, we observed that in all plants, the RCA protein gradually decreased with the onset of dark treatment (Figure 6C). Taken together, these evidences suggest that RCA might

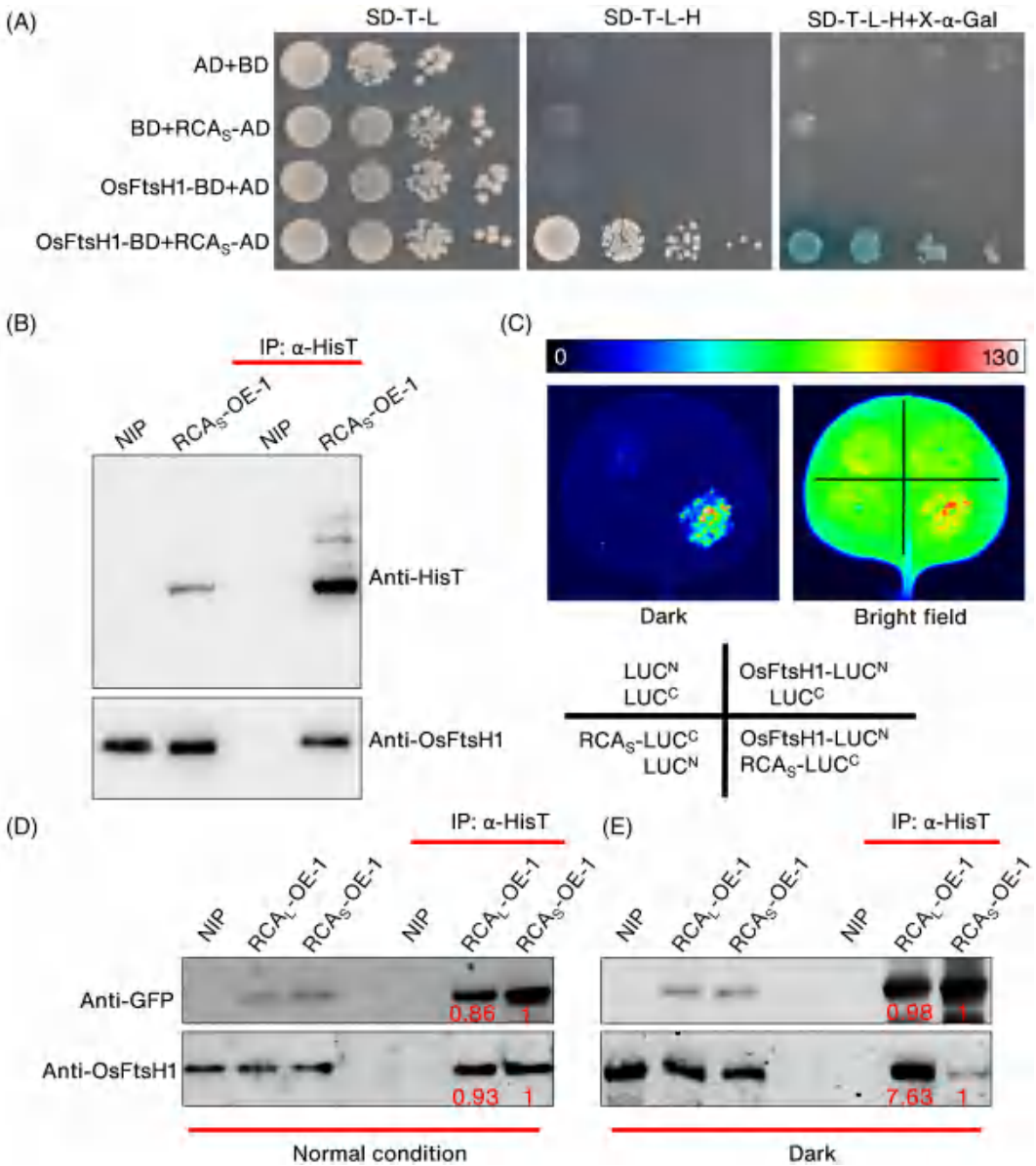


Figure 5. OsFtsH1 is the interacting protein of RCA$_S$.
(A) Y2H showing that OsFtsH1 interacts with RCA$_S$. SD-T-L, SD medium without Leu and Trp; SD-T-L-H, SD medium without Trp, Leu, and His. pGBKT7 + pGADT7, pGBKT7-OsFtsH1+ pGADT7, and pGBKT7 + pGADT7-RCA$_S$ were used as negative controls.
(B) In vivo interaction between OsFtsH1 and RCA$_S$ revealed by the co-immunoprecipitation assay. After immunoprecipitation with anti-HisT, precipitated proteins were probed with an anti-OsFtsH1 antibody.
(C) Firefly luciferase complementation imaging (LCI) assay showing the interaction between RCA$_S$ and OsFtsH1. LUC image of Nicotiana benthamiana leaves co-infiltrated with Agrobacterium strains containing plasmids shown below. LUC$^N$, the firefly LUC fragments of 2–416 amino acids; LUC$^C$, the firefly LUC fragments of 398–550 amino acids. The color bar above shows the range of luminescence intensity in the image. The descriptor below the pictures illustrates the distribution of four combinations of injected Agrobacterium strains.
(D, E) In vivo interaction among OsFtsH1, RCA$_L$-HisT, and RCA$_S$-HisT under normal and dark conditions revealed by the co-immunoprecipitation assay. After immunoprecipitation with anti-HisT beads, precipitated proteins were probed with anti-GFP and anti-OsFtsH1 antibodies. Quantifications (red numbers) were obtained from Image Lab software.

affect the protein stability of OsFtsH1. To test this hypothesis, we further performed cell-free assays by incubating OsFtsH1-GFP-HisT protein purified from Escherichia coli with total proteins extracted from wild-type DJ or rca plants (Figure 6D). The immunoblot assay revealed that the levels of the OsFtsH1-GFP-HisT protein gradually declined in the wild-type plant. In contrast, this decline was mitigated in the rca mutant or upon treatment with MG132 (Figure 6E). These findings suggest that RCA facilitates the degradation of OsFtsH1.

### OsFtsH1 inhibits dark-induced leaf senescence

To further assess the role of OsFtsH1 in RCA-mediated leaf senescence, we generated osftsh1-ami mutants and OsFtsH1-overexpressing plants. Twenty independent transgenic lines were obtained from each transformation, and two lines for single transformants were selected for subsequent experiments. According to the qRT-PCR results, the osftsh1-ami mutant showed a 50% decrease in the transcriptional level of OsFtsH1 compared with the wild type, whereas the OsFtsH1-OE plants showed an approximately fourfold to sixfold increase (Figure S16A). At the protein level, Western blots also confirmed the same results (Figure S16B). We then treated the detached leaves of the osftsh1-ami mutant and OsFtsH1-OE plants in the dark and investigated their senescence phenotypes. As expected, the leaves of OsFtsH1-OE plants showed delayed senescence compared with the leaves of the wild-type and osftsh1-ami mutant plants (Figure 7A). Additionally, OsFtsH1 overexpression significantly increased the chlorophyll content and Fv/Fm ratios (Figure 7B,C). Based on the studies mentioned earlier, we conclude that RCA promotes dark-induced leaf senescence by accelerating the degradation of the OsFtsH1.

## DISCUSSION

Leaf senescence is characterized by the transition from nutrient assimilation to remobilization and has a critical effect on agriculture (Avila-Ospina et al., 2014). However, premature senescence of leaves caused by harsh growth conditions is a critical challenge that causes significant economic losses in terms of crop yield. Although low light causes losses of up to 50% and affects rice yield and quality, its regulatory mechanisms remain poorly understood (Gad et al., 2021). Darkness, an extreme light condition, is often used to induce rapid and synchronous senescence in detached leaves and has been widely used as a senescence model to study the physiological, biochemical, and molecular mechanisms of leaf senescence (Li et al., 2013). In this study, we examined the underlying mechanisms of DIS in intact rice plants and found that RCA, particularly the large isoform $RCA_L$, promotes dark-induced leaf senescence by binding with OsFtsH1.

### $RCA_L$ promotes dark-induced leaf senescence

Previous studies have shown that RCA is involved in many stress responses, suggesting additional roles for RCA beyond RuBisCO regulation (Chen et al., 2015). In C4 grasses, proteomic data suggest that the larger RCA isoform was present at a very low abundance under control conditions, but its expression increased considerably at higher temperatures, allowing for the maintenance of RuBisCO activation, thus indicating a potential thermoprotective role in carbon fixation (Kim et al., 2021). In rice plants, however, our results showed that both $RCA_L$ and $RCA_S$ were markedly downregulated by dark treatment using transcriptomic analysis (Figure S1) and qRT-PCR analysis (Figure 1A). The decline, shown at both the mRNA and protein levels, persisted throughout the dark treatment and natural ageing process (Figure 1B–D), suggesting that RCA is a novel factor involved in the dark stress response.

Dark-induced premature leaf senescence is a well-studied stressor that involves a complex regulatory network. Plant hormones, macromolecular hydrolysis, ROS accumulation, and transcriptional regulation are all involved in DIS (Biswal & Pandey, 2018; Gregersen et al., 2013; Piao et al., 2019; Shim et al., 2019; Zhang et al., 2016). However, in these previously discovered regulatory pathways, researchers have paid more attention to the regulation of SAG expression (Zhang et al., 2022) and the stability of the photosynthetic machinery during abiotic stress (Gururani et al., 2015). In the present study, we found that RCA, an enzyme that regulates photosynthesis by activating RuBisCO, may promote dark-induced leaf senescence. First, rca mutant plants are more tolerant to dark stress (Figure 2). Second, the rca-ami mutant replicated the phenotype of the rca mutant (Figure 2; Figure S8). Third, RCA overexpression caused early dark-induced leaf senescence (Figure 3; Figure S9). In addition, heterologous expression of $RCA_L$ in Arabidopsis reduced basal dark tolerance (Figure S14). Together, these results demonstrate that RCA plays an important role in DIS in rice plants.

### Two RCA isoforms have different roles under dark conditions

Alternative splicing is commonly believed to be a major source of cellular protein diversity and plenty of cases have shown the unique role of protein isoforms (Dong et al., 2018). Differences in the length and abundance of RCA isoforms among plant species have been documented (Salvucci et al., 1987), emphasizing the diversity in their gene and protein isoform production. The large RCA isoform, in its oxidized state, forms a disulfide bond that reduces ATP affinity while increasing sensitivity to ADP inhibition (Shen et al., 1991; Zhang & Portis Jr., 1999). Conversely, the shorter isoform, lacking regulatory cysteines, is less sensitive to ADP inhibition and exhibits no redox regulation. In Arabidopsis, only large isoforms respond to redox regulation due to a C-terminal extension featuring conserved redox-sensing cysteine residues modulated by thioredoxin f (Zhang & Portis Jr., 1999). While Arabidopsis and spinach express the two isoforms in similar amounts (Kim et al., 2016, 2020), rice displays significantly higher levels of small isoforms, both at the mRNA and protein levels (Figure 1), likely due to differing alternative splicing efficiencies. $RCA_L$ is essential for photosynthetic acclimation under moderate stress, while $RCA_S$ primarily maintains RuBisCO activity in normal conditions (Fan

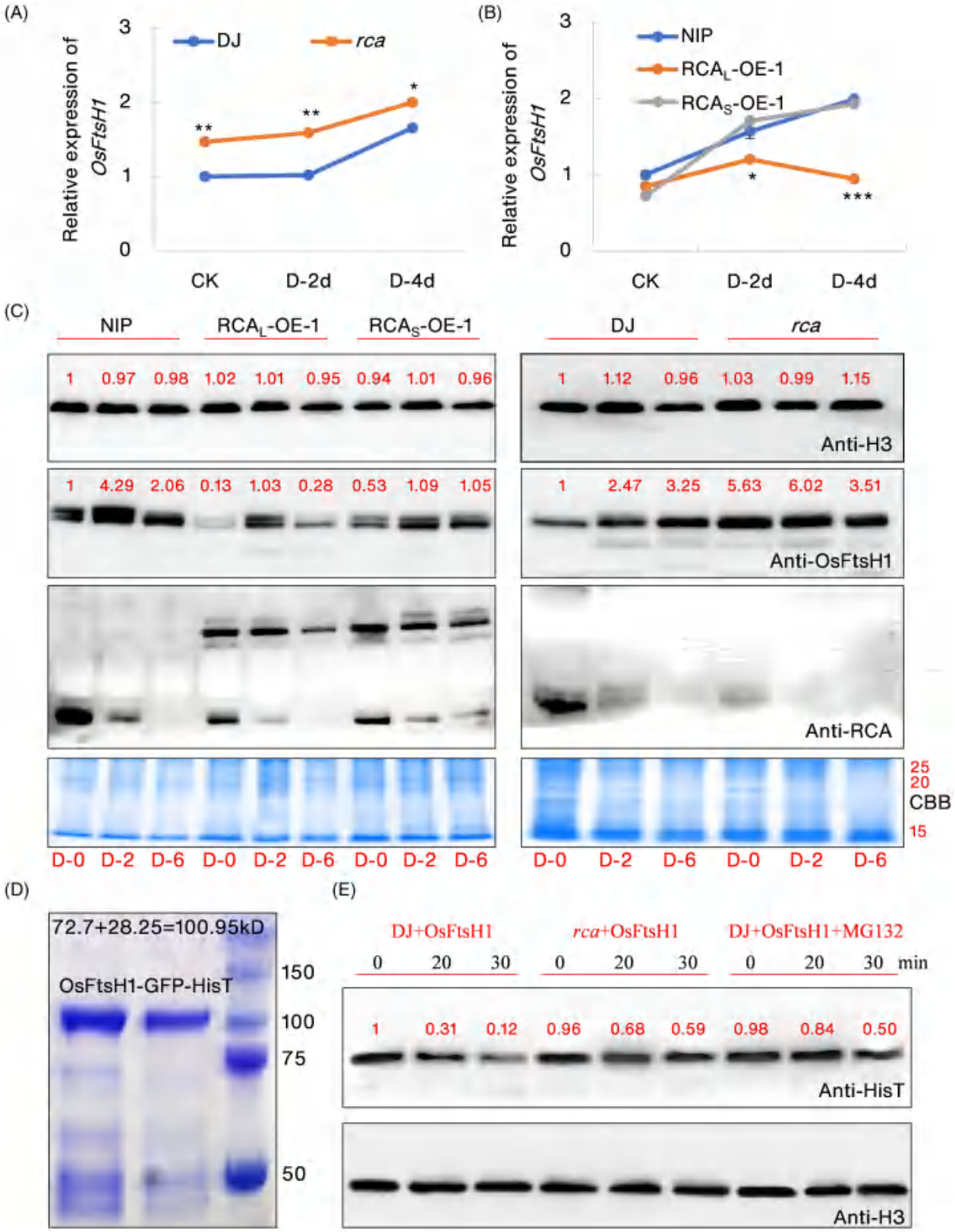

Figure 6. RCA affects the proteolytic degradation of OsFtsH1 protein.
(A, B) Expression level of OsFtsH1 in DJ, rca, NIP, $RCA_L$-OE-1, $RCA_L$-OE-2, $RCA_S$-OE-1, and $RCA_S$-OE-2 plants. Actin was used as the internal control. Expression levels in the wild-type plants were set as "1." Values are presented as means ± SD, and the statistically significant differences were determined by Student's t-test (biological replicates, n = 3, *P < 0.05, **P < 0.01, ***P < 0.001).
(C) Immunoblot analysis of OsFstH1 and RCA in DJ, rca, NIP, $RCA_L$-OE, and $RCA_S$-OE plants upon dark stress (0, 2, and 6 days). Three-week-old seedlings were placed in a completely dark condition, and samples were collected at 0, 2, and 6 days to extract total protein. Equal protein loading was confirmed with the anti-histone H3 antibody and Coomassie Blue staining (CBB). Quantifications (red numbers) were obtained from Image Lab software.
(D) Coomassie blue staining of OsFtsH1-GFP-HisT protein. Both lanes contain the obtained OsFtsH1-GFP-HisT protein.
(E) Promotion of OsFtsH1 degradation by RCA in vitro. OsFtsH1-GFP-HisT protein purified from Escherichia coli was incubated with extracts from DJ or rca plants in the absence or presence of MG132 in cell-free assays. Protein levels were detected at different time points by immunoblotting with anti-HisT antibody. Histone H3 was used as a loading control of plant-extracted proteins. The graph shows the quantitative analysis of protein levels (red numbers). The protein levels at DJ + OsFtsH1-0 were set to "1" as a reference for calculating the relative protein levels.

et al., 2022; Wang et al., 2010). Studies suggest that larger isoforms may facilitate high-temperature acclimation in C4 grasses, showing increased expression with rising temperatures and indicating a thermoprotective role (Kim et al., 2021). However, adaptation strategies vary among grasses; for instance, maize and wheat enhance small isoform expression (Chen et al., 2015). Transgenic plants overexpressing $RCA_L$ display heightened sensitivity to drought stress yet improved thermotolerance, in contrast to $RCA_S$-overexpressing plants, which demonstrate weak drought sensitivity (Salvucci, 2008; Wang et al., 2010). In our study, the functional differences between $RCA_L$ and $RCA_S$ are significant in dark-induced leaf senescence. $RCA_L$ has been shown to play a more prominent role in promoting leaf senescence under dark conditions. This is evidenced by the observation that overexpression of $RCA_L$ accelerates leaf senescence, while $RCA_S$ only exhibits minor effect (Figure 3; Figure S14). In terms of molecular interactions, $RCA_L$ demonstrates a higher binding affinity for OsFtsH1 (Figure 5D,E), a zinc metalloprotease involved in the degradation of proteins within chloroplasts (Liu et al., 2024), thereby affecting the stability of OsFtsH1 during dark stress (Figure 6). In contrast, $RCA_S$ has a minimal effect on the stability of OsFtsH1 and does not significantly contribute to the promotion of senescence (Figures 3 and 6). This distinction highlights the more pronounced role of $RCA_L$ in facilitating OsFtsH1 degradation and its subsequent influence on leaf senescence under dark conditions, while $RCA_S$ appears to play a lesser role in this process.

### OsFtsH1 plays a vital role in dark-induced leaf senescence

Rice contains nine FtsH genes in its genome (Yu et al., 2005), and the function mechanisms of FtsH genes in rice have not been fully understood so far. Among the nine OsFtsH proteins, three (OsFtsH3, OsFtsH4, and OsFtsH5) are expected to be located in the mitochondria, whereas the other six are thought to be found in chloroplasts (Yu et al., 2005; Zhang & Sun, 2009). The hetero-hexametric FtsH complex, consisting of type A and type B subunits, is present in the thylakoid membranes of photosynthetic organisms (Yi et al., 2022). OsFtsH2 is crucial for the development of rice chloroplasts (Wu et al., 2021) and for the regulation of the turnover of cleaved D1 during the booting and seedling stages of chilling tolerance (Liu et al., 2024). In this study, our results suggest that OsFtsH1 is a critical component in the regulation of dark-induced leaf senescence in rice. The role of OsFtsH1 in DIS is underscored by its interaction with RCA, specifically the large isoform $RCA_L$ (Figures 4 and 5). This interaction is pivotal as $RCA_L$ facilitates the degradation of OsFtsH1 (Figure 6), thereby influencing its stability and function during dark stress. Under dark conditions, the expression of RCA is downregulated, leading to a subsequent accumulation of OsFtsH1 (Figures 1C and 6C). This accumulation is critical for maintaining cellular homeostasis and mitigating the adverse effects of dark-induced stress (Figure 7). Furthermore, FtsHs have been identified as having a role in protein turnover and processing and are involved in many biological processes, especially through quality control of the PSII complex (Yi et al., 2022). We speculate that OsFtsH1 may be involved in the degradation of thylakoid membrane proteins such as D1, D2, CP43, and CP47, among others. Further studies will be needed to confirm the interactions between OsFtsH1 and its targets and reveal the mechanisms by which OsFtsH1 participates in dark-induced leaf senescence.

In conclusion, using physiological and molecular analyses, we identified several processes during DIS in rice and demonstrated that RCA is a key positive regulator of these processes; thus, we propose a working model (Figure 8). Under dark conditions, $RCA_L$ is predominantly binding with OsFtsH1 compared to $RCA_S$ and facilitates the degradation of OsFtsH1. On the other hand, dark stress induces a significant decrease in RCA in the RNA expression and protein level. The decline in RCA protein subsequently led to the accumulation and stabilization of OsFtsH1 protein, thereby enabling plants to better withstand extended periods of dark stress. However, in rca mutants, the absence of RCA leads to a reduction in the degradation of OsFtsH1 protein, making the plants more tolerant to dark stress.

## EXPERIMENTAL PROCEDURES

### Phylogenetic analysis of RCA homologous proteins

Sequences of RCA protein orthologs were obtained using BLASTP software available at the NCBI website (http://www.ncbi.nlm.nih.gov/)

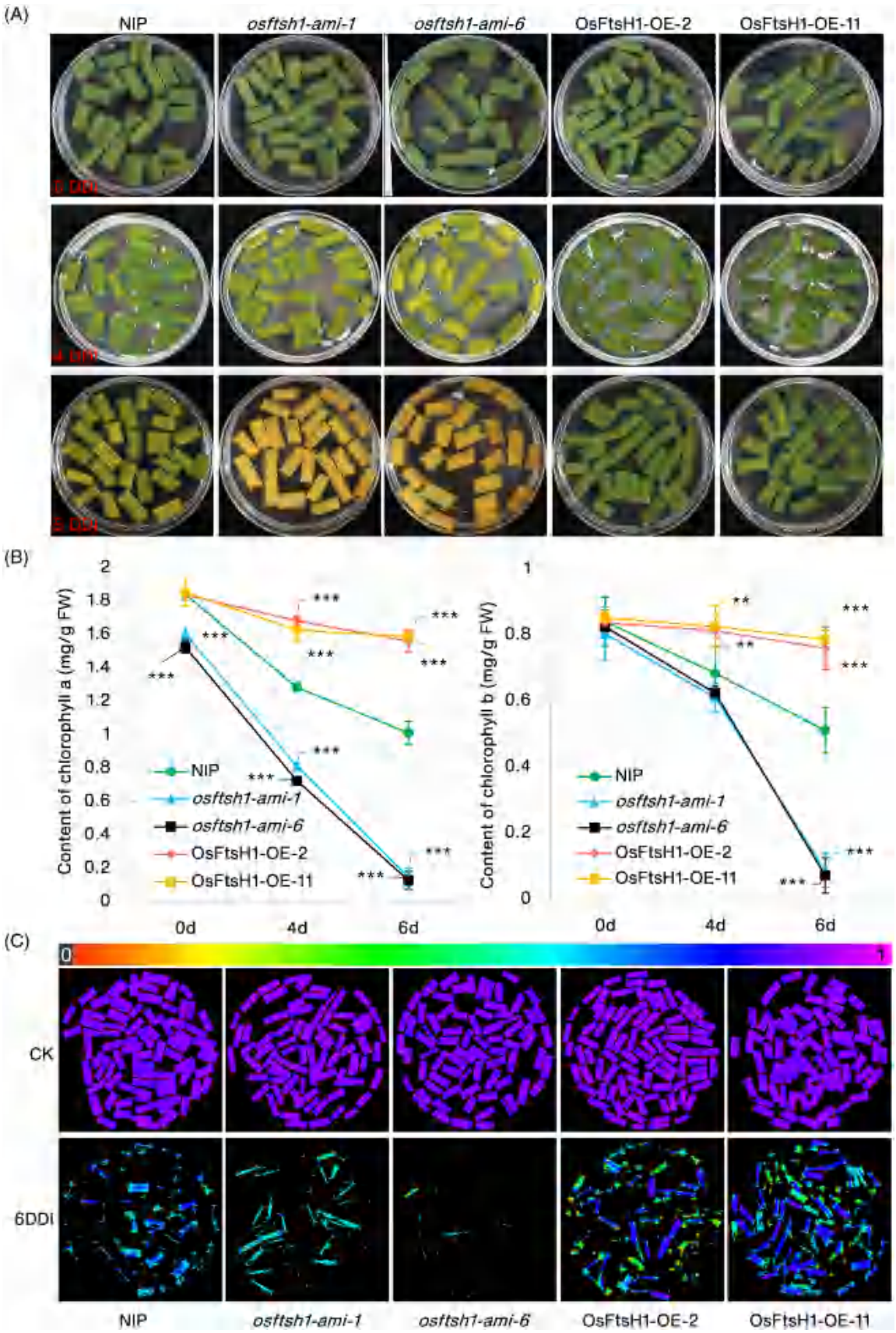

Figure 7. OsFtsH1 inhibits dark-induced leaf senescence.
(A) Leaves of wild-type (NIP), osftsh1-ami, and OsFtsH1-OE plants were treated with darkness for 4 and 6 days and photographed.
(B) Chlorophyll content of wild-type (NIP), osftsh1-ami, and OsFtsH1-OE plants. Values were presented as means ± SD, and the statistically significant differences were determined by Student's t-test (biological replicates, n = 20, **P < 0.01, ***P < 0.001, compared with the wild type).
(C) Fv/Fm images of wild-type (NIP), osftsh1-ami, and OsFtsH1-OE plants obtained using the PlantView230F imaging system under normal conditions and dark treatment.

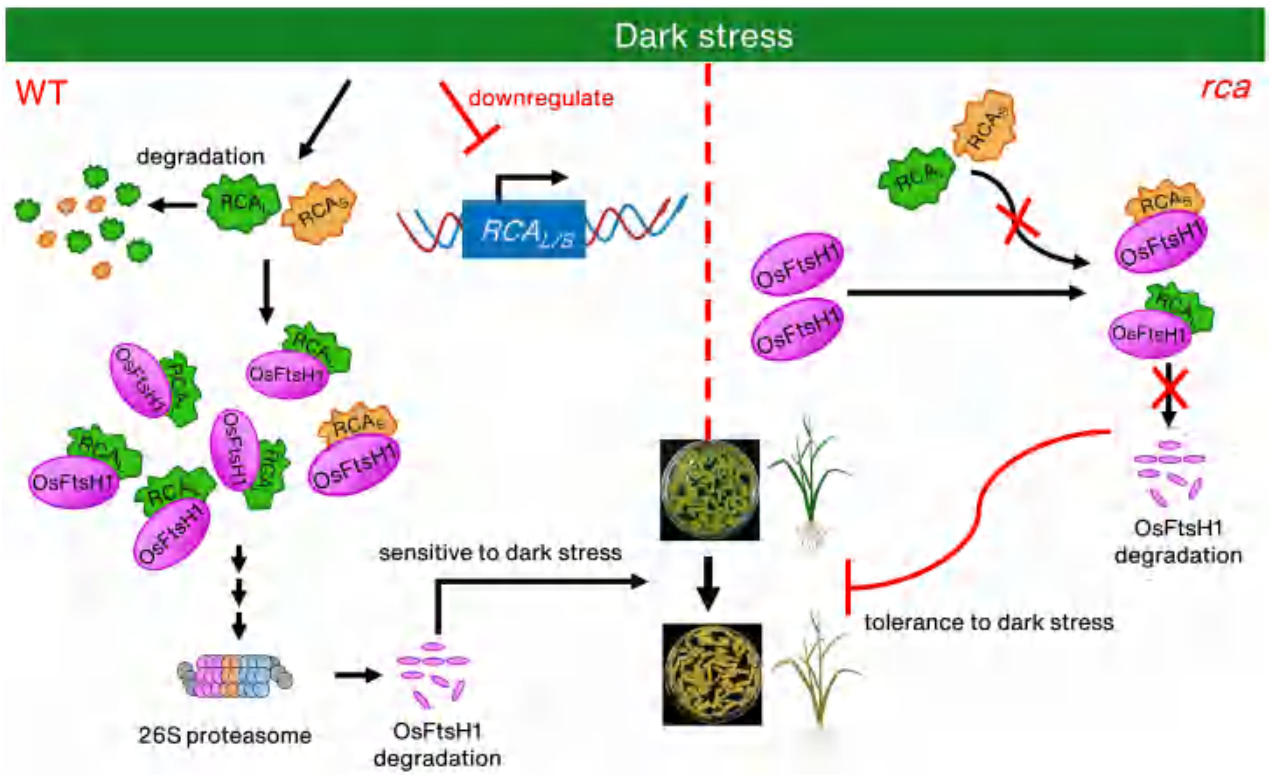


Figure 8. Proposed model depiction of the key role of RCA in dark-induced senescence.
RCA is a positive regulator in dark-induced senescence. On the one hand, dark stress inhibits the transcription of the RCA gene and also promotes the degradation of RCA protein. On the other hand, OsFtsH1, as an interacting protein of $RCA_L$ and $RCA_S$, negatively regulates the senescence induced by dark stress. Under dark stress, OsFtsH1 is more likely to form a complex with $RCA_L$ than with $RCA_S$ protein, which accelerates the degradation of OsFtsH1 and ultimately leads to the acceleration of senescence.

and UniProt website (https://www.uniprot.org/). BLASTP analyses were performed against the protein databases of monocotyledons, dicotyledons, and algae. Clustal alignment was used to align the 32 RCA proteins, and the neighbor-joining approach was used to determine evolutionary history (Chen et al., 2021). Thirty-two amino acid sequences were analyzed. All positions with missing data and gaps were removed. MEGA7.0 was used to perform evolutionary analyses (Kumar et al., 2016). Phylogenetic analysis was performed using FASTTREE (http://www.microbesonline.org/fasttree/) (Zhao et al., 2019). The conserved domain of RCA protein was predicted using the NCBI conserved domain database (https://www.ncbi.nlm.nih.gov/cdd).

## Sequences analysis

Rice RCA protein sequences were obtained from the Rice Genome Annotation Project Database (http://rice.plantbiology.msu.edu/). RCA sequences from other species (N. tabacum, Ipomoea batatas, Spinacia oleracea, Arabidopsis thaliana, Brassica oleracea, Cucumis sativus, Helianthus annuus, Phaseolus vulgaris, Vigna radiata, Glycine max, Z. mays, S. bicolor, H. vulgare, T. aestivum, P. australis, A. pyrenoidosa, and Chlamydomonas reinhardtii) were collected from UniProt (https://www.uniprot.org/). All the sequences were aligned using Clustal Omega (https://www.ebi.ac.uk/Tools/msa/clustalo/). $AAA^+$ domains selected from the representative species were aligned using JALVIEW software with MAFFT and LOGO analyses (Chen et al., 2021).

## Plant material and growth conditions

Wild-type (Dongjin) and T-DNA insertional mutant (rca) plants were obtained from the Crop Biotech Institute of Kyung Hee University (Seoul, Korea) (Jeon et al., 2000; Jeong et al., 2006). rca-ami and osftsh1-ami plants were generated using amiRNAs, as described previously (Schwab et al., 2006). The target sequences of RCA (5′-tagtcgtacgttctcagaccc-3′) and OsFtsH1 (5′-ttgctataatcctaaccgcca-3′) were cloned into the pBWA(V)HS-ccdB-ami vector and subsequently inserted into NIP rice calli by Agrobacterium (EHA105)-mediated transformation. Twenty independent lines

were obtained for each transformation. Genomic DNA was extracted from transgenic plants and amplified by PCR for genotyping (Table S2); two of these were used in the subsequent analysis.

The rice seeds were sterilized with 95% ethyl alcohol and washed five times with sterile water. The sterilized seeds were soaked in water for 2 days, and the uniformly germinated seeds were sown in bottomless 96-well PCR plates with appropriate spacing in the nutrient solution. They were then grown at 30°C under white light at approximately 50 lmol $m^{-2}$ $sec^{-1}$ for 14 h and then at 25°C in a dark cycle for 10 h in a growth chamber (Zhang et al., 2023).

A. thaliana ecotype Col-0 was used in this work. The mutants (SALK_003204) were obtained from the Arabidopsis Biological Resource Center, and homozygous mutants were collected by genotyping with the primers listed in Table S2. After sterilization in 70% ethanol for 3 min, Arabidopsis seeds were rinsed three times with sterile water and placed on 1/2 Murashige and Skoog medium plates supplemented with 1% sucrose. The seeds were then stratified at 4°C for 2 days in the dark before being moved into continuous light conditions for germination. The seeds were then grown under a 16-h light (23–25°C)/8-h dark (17–20°C) photoperiod. Plants were grown in soil under the same photoperiod.

## Transcriptome sequencing and KEGG enrichment analysis

Total RNA was extracted from 30-day-old wild-type plants under normal growth conditions and after 4 h of dark treatment. Sequencing was performed on a Gene$^{+}$Seq-2000 sequencing system (GenePlus, Beijing, China) with 100-bp paired-end reads, according to the manufacturer's recommendations. The raw reads were further processed using a bioinformatics pipelinetool GenePlus Cloud (https://www.jyjcloud.com/) online platform. Quantification of gene expression levels was performed using FPKM (fragments per kilobase of transcript per million mapped fragments). The dataset was filtered to retain only genes with FPKM >2 in at least two samples, thus removing genes that were not expressed or expressed at a very low level. The quantitative transcriptome results were analyzed via difference analysis to obtain the log2(fold change) and P-value of different statistical tests for the relative expression of the transcriptome in each comparison group. Differentially regulated transcripts were defined as |log2 (fold change)| ≥1 and a P-value (Padj, P values corrected for multiple testing) ≤1e-10. Differential expression between the two groups was analyzed using DESeq2 (Chen et al., 2023). For KEGG pathway enrichment analysis, the DEGs were first mapped to the KEGG pathway term in the UniProt ID mapping database (https://www.uniprot.org/id-mapping). Then, KEGG Mapper-Search website (https://www.kegg.jp/kegg/mapper/) was applied to find pathways that were significantly enriched in the candidate gene map with respect to the entire genome background (Kanehisa & Sato, 2020).

## Purification of fusion protein and generation of antibody

Using the primers listed in Table S2, the RCA fragment (AA:1–428, removed chloroplast transit peptide) was amplified from NIP cDNA. The fragments were digested with BamHI and HindIII and then introduced into the pET30a expression vectors for protein expression in the E. coli BL21 (DE3) strain. OsFtsH1 fragments from NIP cDNA were inserted into pET30a-GFP vector for His-GFP-tagged protein after EcoRI and BamHI digestion and expressed in the E. coli Transetta (DE3) strain (Zhang et al., 2021). After reaching an OD600 of 0.6 at 37°C, the cells were incubated overnight at 24°C using 0.2 mmol $L^{-1}$ IPTG (isopropyl b-D-thiogalactoside). Cultures were collected by centrifugation, resuspended in binding buffer (40 mM PBS, pH 7.4), and purified using Ni-NTA His-bind resin. Protein concentrations were calculated using Bradford reagent (Bio-Rad) and bovine serum albumin (BSA) as a reference (Zhang et al., 2023).

A polyclonal antibody against RCA was raised in the rabbit at Wuhan Genecreate Biological Engineering Co., Ltd. In total, 500 mg of a polypeptide (GDANSDAMKTGSFYG) was used for the initial immunization, and 250 mg of the same polypeptide was used for each of the next three booster shots. For western blotting, antibodies were used at a dilution of 1:300. The antibody was verified using the purified protein described earlier.

## Immunoblot assays

The total protein content of rice seedlings was extracted using an extraction buffer containing 50 mM Tris pH 6.8, 4% SDS, 10% glycerol, 5% 2-mercaptoethanol, 20% bromophenol blue, and a complete protease inhibitor (Sigma). Cellular debris was removed by centrifugation at 4°C, and the supernatant concentration was quantified using the Bradford assay with BSA as a standard. All samples were adjusted to the same concentration for the immunoblot assay. Proteins were separated using 12% SDS-PAGE and transferred onto polyvinylidene fluoride (PVDF) membranes, and then, the PVDF membrane was blocked with 5% milk in Tris-buffered saline with Tween-20 (TBST) (0.8% NaCl, 0.02% KCl, 0.3% Tris, pH 7.4, and 0.05% Tween 20) for an hour at room temperature. Excess milk was washed off with TBST. Primary antibodies were applied to the blots and incubated for 2 h at room temperature. In this investigation, six polyclonal antibodies (1:5000 dilution) were used: anti-histone H3 (ab1791; Abcam), anti-actin (ABM40122; Abbkine), anti-FtsH1 (PHY1823S; PHYTOAB), anti-GFP (G6539; Roche), anti-His (CW0286; CWBIO), and anti-GST (CW0088M; CWBIO). The secondary antibodies were applied for an hour at room temperature. Blots were developed with ECL chemiluminescence detection solutions (Invitrogen), and the ChemiDoc system (Bio-Rad) was used to detect the results. Actin and histone H3 were used as the internal controls.

## RNA isolation, semi-quantitative RT-PCR, and RT-PCR

To determine gene expression, total RNA was extracted using TRIzol reagent (Invitrogen) according to the manufacturer's instructions. Following the manufacturer's instructions, RNA samples were reverse transcribed using TOROBlue® qRT Premix with gDNA Eraser 2.0 (TOYOBO), and qRT-PCR was performed on a qRT-PCR system (CFX96; Bio-Rad) using SYBR Premix (TaKaRa). Semi-quantitative RT-PCR was performed using 1 lL cDNA as a template (Karmakar et al., 2017). The relative expression of the target gene was normalized to that of rice OsActin1 (LOC_Os03g50885) or histone H3 (Os06g0160001). All the primers used for qRT-PCR and semi-quantitative RT-PCR are listed in Table S2.

## Vector construction and rice transformation

The ubiquitin promoter, eGFP fragment, and NOS Terminator were amplified from pGA3427 (Kim et al., 2009), digested with EcoRI and XmaI, and inserted into pCAMBIA2300 to generate the pUbi::GFP-pCAMBIA2300 vector. The ORFs of $RCA_L$, $RCA_S$, and OsFtsH1 were cloned into pUbi::GFP-pCAMBIA2300 vector with MluI and SpeI digestion and introduced into NIP rice calli by Agrobacterium (EHA105)-mediated transformation, respectively. At least 20 independent lines were obtained for each transformation. Genomic DNA was extracted from transgenic plants and amplified

by PCR for genotyping (Table S2), two of which were used for further investigation.

### Subcellular localization

Vectors were constructed as described previously to investigate the subcellular localization of $RCA_L$ and $RCA_S$. For co-localization of $RCA_L$ and OsFtsH1, the ORF of OsFtsH1 was amplified by PCR and inserted into the pCAMBIA1300-35S-mcherry vector. The primers used are listed in Table S2. The construct was transiently expressed in protoplasts of NIP and $RCA_L$-OE plant cell suspensions by polyethylene glycol-mediated transformation. Fluorescence signals were visualized using a confocal laser-scanning microscope (LSM710, Carl Zeiss, Germany) (Wang et al., 2022).

### DIS

Detachable fully developed flag leaves were taken from 3-week-old rice plants and placed with the abaxial side facing upward in an incubator with 3 mM MES buffer (pH 5.8) at 27°C for 4 or 8 days under dark conditions (Suzuki et al., 2021). Whole rice plants were grown for 1 month under normal conditions for the DIS tests, after which they were placed in the dark at 28°C for 10 days (Shim et al., 2020). The chlorophyll content of the flag leaves was determined.

### Chlorophyll fluorescence analysis and determination of chlorophyll content

For detached leaves, Fv/Fm images and Fv/Fm ratios were obtained using a PlantView230F Imaging System (BLT, Guangzhou, China). For dark tolerance experiments, the plants were exposed to darkness for the indicated times, and then, fully expanded flag leaves were detected. For chlorophyll determination, equal weights of freshly harvested, fully expanded flag leaves from seedlings that were 5, 7, and 10 days old were marinated in 95% ethanol for 48 h under dark conditions. The residual plant debris was removed by centrifugation. The supernatants of these samples were then analyzed using a spectrophotometer (RUNQEE, Shanghai, China), and the quantities of chlorophylls were measured at 663 and 645 nm (Cho et al., 2018).

### DAB staining

One-month-old rice seedlings were transferred to darkness at 28°C for 6 days, and the leaves were harvested and treated in 1 mg $mL^{-1}$ DAB (3,3′-diaminobenzidine) solution for 4 h to detect the cellular $H_2O_2$ following straining. The leaves were triple washed with $ddH_2O$, incubated and decolorized in 75% ethanol for 24 h, and then photographed (Zhang et al., 2018).

### Co-IP and mass spectrometry analysis

Co-IP was performed as previously reported, with minor modifications (Li et al., 2018). The total protein of wild-type, $RCA_L$-OE, and $RCA_S$-OE plants was extracted using 1 g of each sample with 2.5 mL extraction buffer containing 50 mM Tris pH 7.6, 150 mM NaCl, 5 mM $MgCl_2$, 10% glycerol, and a complete protease inhibitor (Sigma). Proteins were immunoprecipitated using 40 lL of BeyoMag™ Anti-GFP Magnetic Beads (Beytime) for 3 h at 4°C, and the immunoprecipitates were eluded with 40 lL loading buffer [0.5 M Tris pH 6.8, 2% (w/v) SDS, 5% (v/w) glycerol, 2.5% (v/v) 2-mercaptoethanol, and 10% (v/w) bromophenol blue]. Twenty microliter samples were separated using SDS-PAGE. After release from the bead-bound complex, protein levels were measured using western blotting. For proteomic analysis, LC–MS/MS detection was performed using a hybrid quadrupole time-of-flight LC–MS/MS mass spectrometer. MS/MS analysis was performed using ProteinPilot Software 5.0, and amino acid sequences from the UniProt rice protein database were used to analyze the MS/MS-acquired data.

For Co-IP assay performed in N. benthamiana leaves, full-length OsFtsH1 and $RCA_L$ were amplified and inserted into pUbi::GFP-pCAMBIA2300 and pCAMBIA1300-cLUC vectors, respectively. The resulting transient expression constructs were transformed into GV3101. After incubation for 2 days, 1 g of sample was used to extract protein with 2.5 mL extraction buffer (25 mM Tris–HCl, pH 7.5, 1 mM EDTA, 150 mM NaCl, 10% glycerol, and 5 mM dithiothreitol) in the presence of protease inhibitor cocktail (Sigma). After immunoprecipitation with anti-GFP Magnetic Beads, precipitated proteins were eluded with 40 lL loading buffer. Twenty microliter samples were used for loading and testing. Their interaction was detected by an anti-RCA antibody.

### Experiments to validate protein–protein interactions

For the Y2H assays, the ORFs of the two interacting genes were individually inserted into the pGBKT7 and pGADT7 vectors. The bait and prey plasmids were transformed into yeast strain AH109. To examine protein interactions, yeast colonies were patched in duplicate onto synthetic dropout Trp-Leu (SD-T-L), SD-T-L-H (SD-T-L-H), and SD-T-L-H + X-a-Gal plates, which were then incubated at 30°C for 2–3 days.

For BiFC assays, the pDOE-03 BiFC vector was adopted for the BiFC assays (Gookin & Assmann, 2014). The CDS of RCA without stop codon was ligated into multiple cloning site 3 of the pDOE-03 plasmid to create a "parent" vector. The CDS of OsFtsH1 was inserted into multiple cloning site 1 of the pDOE-03 plasmid and parent vector. The above vectors were transformed into Agrobacterium strain GV3101 and then infiltrated into N. benthamiana leaves for the BiFC assay. After 48 h of incubation, the transformed leaves were observed for yellow fluorescence using a Zeiss LSM710 confocal laser scanning microscope (Carl Zeiss, Germany). The laser is 514 nm, intensity is 2.0%, collection bandwidth is 519–576 nm, and master gain is 682.

For LCI assays, the coding sequences of $RCA_S$ and OsFtsH1 were amplified and cloned into the pCAMBIA1300-$LUC^C$ and pCAMBIA1300-$LUC^N$ vectors, respectively. Agrobacterium tumefaciens (GV3101) bacteria bearing the above constructs were infiltrated into N. benthamiana leaves, and the leaves were subsequently covered with plastic for 2 days and exposed to light again for 16 h. LUC images were obtained using a low-light, cooled CCD imaging system (ROPER CA2048B; ROPER Scientific) (Wu et al., 2023).

### Vector construction and Arabidopsis transformation

To further verify the function of RCA protein, the $RCA_L$ and $RCA_S$ segments were inserted into pCAMBIA2300-GFP with MluI and SpeI digestion. The resulting plasmids were transformed into Atrca mutants using Agrobacterium strain GV3101 via floral dipping (Hsu et al., 2022). At least 10 independent lines were obtained, and two of them were used for further study.

### Protein degradation assay

In vitro OsFtsH1 degradation assays were performed as described previously with some modifications (Wang et al., 2020). Briefly, total proteins of DJ and rca plants were extracted in buffer containing 50 mM Tris-HCl (pH 8.0), 500 mM sucrose, 1 mM MgCl2,10 mM EDTA (pH 8.0), and 1 mM DTT. Then, the extracted total proteins were incubated with OsFtsH1-GFP-HisT protein

purified from E. coli under dark at 30°C with or without 50 mM MG132 in different time gradients. After incubation, 10 ⅼL sample was loaded for both immunoblot, and anti-HisT antibody was used to detect the OsFtsH1 protein.

## ACCESSION NUMBERS

Sequence data from this article can be found in the Rice Genome Annotation Project database and The Arabidopsis Information Resource database under the following accession numbers: RCA (LOC_Os11g47970), OsFtsH1 (LOC_Os06g51029), SGR (LOC_Os09g36200), NAP (LOC_Os03g21060), H3 (Os06g0160001), OsACTIN1 (LOC_Os03g50885), AtRCA (At2g39730), and AtACTIN7 (At5g09810).

## AUTHOR CONTRIBUTIONS

YanliZ, JW, QQ, and YY conceived and designed the research. YingZ, XW, BR, YJ, LL, and FC conducted experiments. YanliZ, LW, JW, Y-WY, and YY analyzed data and wrote the manuscript. All authors read and approved the manuscript.

## ACKNOWLEDGMENTS

This work was supported by funds from the National Natural Science Foundation of China (32370328 to LW), the High-Level Talent Special Support Program of Zhejiang Province (YY), and the Natural Science Foundation of Zhejiang (LY23C130001 to BR). We thank LetPub (www.letpub.com.cn) for its linguistic assistance during the preparation of this manuscript.

## CONFLICT OF INTEREST STATEMENT

The authors declare that they have no conflict of interest.

## DATA AVAILABILITY STATEMENT

The data that support the findings of this study are available from the corresponding author upon reasonable request.

## SUPPORTING INFORMATION

Additional Supporting Information may be found in the online version of this article.

Figure S1. DIS transcriptomic analysis.

Figure S2. Antibody of RCA protein.

Figure S3. Phylogenetic trees and conserved domain of RCA proteins.

Figure S4. Multiple alignments of RCA proteins.

Figure S5. rca mutants display morphological defects.

Figure S6. Chlorophyll content in DJ and rca leaves at different periods.

Figure S7. rca displayed delayed dark-induced leaf senescence.

Figure S8. rca-ami displayed delayed dark-induced leaf senescence.

Figure S9. Confirmation of RCA overexpression plants.

Figure S10. Gross morphology and expression level of senescence-associated gene.

Figure S11. RCA reduces tolerance to prolonged darkness.

Figure S12. T-DNA mutant of AtRCA.

Figure S13. Relative expression and protein level in the transgenic Arabidopsis.

Figure S14. RCA is involved in dark-induced senescence in Arabidopsis.

Figure S15. OsFtsH1 is the interacting protein of $RCA_L$.

Figure S16. osftsh1-ami and OsFtsH1-OE plants.

Table S2. A list of primers used in this study.

Table S1. Differentially expressed genes between NIP-CK and NIP-D.

## REFERENCES

Avila-Ospina, L., Moison, M., Yoshimoto, K. & Masclaux-Daubresse, C. (2014) Autophagy, plant senescence, and nutrient recycling. Journal of Experimental Botany, 65, 3799–3811.

Biswal, B. & Pandey, J.K. (2018) Loss of photosynthesis signals a metabolic reprogramming to sustain sugar homeostasis during senescence of green leaves: role of cell wall hydrolases. Photosynthetica, 56, 404–410.

Bracher, A., Whitney, S.M., Hartl, F.U. & Hayer-Hartl, M. (2017) Biogenesis and metabolic maintenance of Rubisco. Annual Review of Plant Biology, 68, 29–60.

Chen, C.J., Wu, Y., Li, J.W., Wang, X., Zeng, Z.H., Xu, J. et al. (2023) TBtools-II: a "one for all, all for one" bioinformatics platform for biological big-data mining. Molecular Plant, 16, 1733–1742.

Chen, F., Dong, G., Wang, F., Shi, Y., Zhu, J., Zhang, Y. et al. (2021) A beta-ketoacyl carrier protein reductase confers heat tolerance via the regulation of fatty acid biosynthesis and stress signaling in rice. The New Phytologist, 232, 655–672.

Chen, Y., Wang, X.M., Zhou, L., He, Y., Wang, D., Qi, Y.H. et al. (2015) Rubisco activase is also a multiple responder to abiotic stresses in rice. PLoS One, 10, e0140934.

Cho, S.H., Lee, C.H., Gi, E., Yim, Y., Koh, H.J., Kang, K. et al. (2018) The rice rolled fine striped (RFS) CHD3/Mi-2 chromatin remodeling factor epigenetically regulates genes involved in oxidative stress responses during leaf development. Frontiers in Plant Science, 9, 364.

Dong, C., He, F., Berkowitz, O., Liu, J., Cao, P., Tang, M. et al. (2018) Alternative splicing plays a critical role in maintaining mineral nutrient homeostasis in rice (Oryza sativa). Plant Cell, 30, 2267–2285.

Fan, X., Liu, J., Zhang, Z., Xi, Y., Li, S., Xiong, L. et al. (2022) A long transcript mutant of the rubisco activase gene RCA upregulated by the transcription factor Ghd2 enhances drought tolerance in rice. The Plant Journal, 110, 673–687.

Flecken, M., Wang, H., Popilka, L., Hartl, F.U., Bracher, A. & Hayer-Hartl, M. (2020) Dual functions of a Rubisco activase in metabolic repair and recruitment to carboxysomes. Cell, 183, 457–473.e20.

Fukao, T., Yeung, E. & Bailey-Serres, J. (2012) The submergence tolerance gene SUB1A delays leaf senescence under prolonged darkness through hormonal regulation in rice. Plant Physiology, 160, 1795–1807.

Gad, A.G., Habiba, Zheng, X. & Miao, Y. (2021) Low light/darkness as stressors of multifactor-induced senescence in rice plants. International Journal of Molecular Sciences, 22, 3936.

Gao, Q., Yang, Z., Zhou, Y., Yin, Z., Qiu, J., Liang, G. et al. (2012) Characterization of an Abc1 kinase family gene OsABC1-2 conferring enhanced tolerance to dark-induced stress in rice. Gene, 498, 155–163.

Gookin, T.E. & Assmann, S.M. (2014) Significant reduction of BiFC non-specific assembly facilitates in planta assessment of heterotrimeric G-protein interactors. The Plant Journal, 80, 553–567.

Gregersen, P.L., Culetic, A., Boschian, L. & Krupinska, K. (2013) Plant senescence and crop productivity. Plant Molecular Biology, 82, 603–622.

Guo, Y. & Gan, S.S. (2012) Convergence and divergence in gene expression profiles induced by leaf senescence and 27 senescence-promoting hormonal, pathological and environmental stress treatments. Plant, Cell & Environment, 35, 644–655.

Gururani, M.A., Venkatesh, J. & Tran, L.S. (2015) Regulation of photosynthesis during abiotic stress-induced photoinhibition. Molecular Plant, 8, 1304–1320.

Habiba, Xu, J., Gad, A.G., Luo, Y., Fan, C., Uddin, J.B.G. et al. (2021) Five OsS40 family members are identified as senescence-related genes in rice by reverse genetics approach. Frontiers in Plant Science, 12, 701529.

Have, M., Marmagne, A., Chardon, F. & Masclaux-Daubresse, C. (2017) Nitrogen remobilization during leaf senescence: lessons from Arabidopsis to crops. Journal of Experimental Botany, 68, 2513–2529.

Hortensteiner, S. & Feller, U. (2002) Nitrogen metabolism and remobilization during senescence. Journal of Experimental Botany, 53, 927–937.

Hsu, C.Y., Chou, M.L., Wei, W.C., Chung, Y.C., Loo, X.Y. & Lin, L.F. (2022) Chloroplast protein Tic55 involved in dark-induced senescence through AtbHLH/AtWRKY-ANAC003 controlling pathway of Arabidopsis thaliana. Genes (Basel), 13, 308.

Jan, S., Abbas, N., Ashraf, M. & Ahmad, P. (2019) Roles of potential plant hormones and transcription factors in controlling leaf senescence and drought tolerance. Protoplasma, 256, 313–329.

Jeon, J.S., Lee, S., Jung, K.H., Jun, S.H., Jeong, D.H., Lee, J. et al. (2000) T-DNA insertional mutagenesis for functional genomics in rice. The Plant Journal, 22, 561–570.

Jeong, D.H., An, S., Park, S., Kang, H.G., Park, G.G., Kim, S.R. et al. (2006) Generation of a flanking sequence-tag database for activation-tagging lines in japonica rice. The Plant Journal, 45, 123–132.

Ji, K., Wang, Y., Sun, W., Lou, Q., Mei, H., Shen, S. et al. (2012) Drought-responsive mechanisms in rice genotypes with contrasting drought tolerance during reproductive stage. Journal of Plant Physiology, 169, 336–344.

Jibran, R., Hunter, D.A. & Dijkwel, P.P. (2013) Hormonal regulation of leaf senescence through integration of developmental and stress signals. Plant Molecular Biology, 82, 547–561.

Jin, J., Duan, J., Shan, C., Mei, Z., Chen, H., Feng, H. et al. (2020) Ethylene insensitive3-like2 (OsEIL2) confers stress sensitivity by regulating OsBURP16, the beta subunit of polygalacturonase (PG1beta-like) subfamily gene in rice. Plant Science, 292, 110353.

Jin, S.H., Hong, J., Li, X.Q. & Jiang, D.A. (2006) Antisense inhibition of Rubisco activase increases Rubisco content and alters the proportion of Rubisco activase in stroma and thylakoids in chloroplasts of rice leaves. Annals of Botany, 97, 739–744.

Kanehisa, M. & Sato, Y. (2020) KEGG mapper for inferring cellular functions from protein sequences. Protein Science, 29, 28–35.

Karmakar, S., Molla, K.A., Das, K., Sarkar, S.N., Datta, S.K. & Datta, K. (2017) Dual gene expression cassette is superior than single gene cassette for enhancing sheath blight tolerance in transgenic rice. Scientific Reports, 7, 7900.

Kato, Y., Hyodo, K. & Sakamoto, W. (2018) The photosystem ii repair cycle requires FtsH turnover through the EngA GTPase. Plant Physiology, 178, 596–611.

Kato, Y., Kuroda, H., Ozawa, S.I., Saito, K., Dogra, V., Scholz, M. et al. (2023) Characterization of tryptophan oxidation affecting D1 degradation by FtsH in the photosystem II quality control of chloroplasts. eLife, 12, RP88822.

Keech, O., Pesquet, E., Gutierrez, L., Ahad, A., Bellini, C., Smith, S.M. et al. (2010) Leaf senescence is accompanied by an early disruption of the microtubule network in Arabidopsis. Plant Physiology, 154, 1710–1720.

Kim, S.R., Lee, D.Y., Yang, J.I., Moon, S. & An, G. (2009) Cloning vectors for rice. Journal of Plant Biology, 52, 73–78.

Kim, S.Y., Bender, K.W., Walker, B.J., Zielinski, R.E., Spalding, M.H., Ort, D.R. et al. (2016) The plastid casein kinase 2 phosphorylates Rubisco activase at the Thr-78 site but is not essential for regulation of Rubisco activation state. Frontiers in Plant Science, 7, 404.

Kim, S.Y., Slattery, R.A. & Ort, D.R. (2021) A role for differential Rubisco activase isoform expression in C4 bioenergy grasses at high temperature. GCB Bioenergy, 13, 211–223.

Kim, S.Y., Stessman, D.J., Wright, D.A., Spalding, M.H., Huber, S.C. & Ort, D.R. (2020) Arabidopsis plants expressing only the redox-regulated Rca-alpha isoform have constrained photosynthesis and plant growth. The Plant Journal, 103, 2250–2262.

Kim, T., Kang, K., Kim, S.H., An, G. & Paek, N.C. (2019) OsWRKY5 promotes rice leaf senescence via senescence-associated NAC and abscisic acid biosynthesis pathway. International Journal of Molecular Sciences, 20, 4437.

Krynicka, V., Skotnicova, P., Jackson, P.J., Barnett, S., Yu, J., Wysocka, A. et al. (2023) FtsH4 protease controls biogenesis of the PSII complex by dual regulation of high light-inducible proteins. Plant Communications, 4, 100502.

Kumar, S., Stecher, G. & Tamura, K. (2016) MEGA7: molecular evolutionary genetics analysis version 7.0 for bigger datasets. Molecular Biology and Evolution, 33, 1870–1874.

Lakshmanan, M., Lim, S.H., Mohanty, B., Kim, J.K., Ha, S.H. & Lee, D.Y. (2015) Unraveling the light-specific metabolic and regulatory signatures of rice through combined in silico modeling and multiomics analysis. Plant Physiology, 169, 3002–3020.

Li, D., Song, H., Mei, H., Fang, E., Wang, X., Yang, F. et al. (2018) Armadillo repeat containing 12 promotes neuroblastoma progression through interaction with retinoblastoma binding protein 4. Nature Communications, 9, 2829.

Li, Z., Peng, J., Wen, X. & Guo, H. (2013) Ethylene-insensitive3 is a senescence-associated gene that accelerates age-dependent leaf senescence by directly repressing miR164 transcription in Arabidopsis. Plant Cell, 25, 3311–3328.

Li, Z., Zhang, Y., Zou, D., Zhao, Y., Wang, H.L., Zhang, Y. et al. (2020) LSD 3.0: a comprehensive resource for the leaf senescence research community. Nucleic Acids Research, 48, D1069–D1075.

Liebsch, D. & Keech, O. (2016) Dark-induced leaf senescence: new insights into a complex light-dependent regulatory pathway. The New Phytologist, 212, 563–570.

Liu, D., Luo, S., Li, Z., Liang, G., Guo, Y., Xu, Y. et al. (2024) COG3 confers the chilling tolerance to mediate OsFtsH2-D1 module in rice. The New Phytologist, 241, 2143–2157.

Mei, Q., Yang, Y., Ye, S., Liang, W., Wang, X., Zhou, J. et al. (2019) $H_2O_2$ induces association of RCA with the thylakoid membrane to enhance resistance of Oryza meyeriana to Xanthomonas oryzae pv. oryzae. Plants (Basel), 8, 351.

Miziorko, H.M. & Lorimer, G.H. (1983) Ribulose-1,5-bisphosphate carboxylase-oxygenase. Annual Review of Biochemistry, 52, 507–535.

Nagarajan, R. & Gill, K.S. (2018) Evolution of Rubisco activase gene in plants. Plant molecular biology, 96, 69-87.

Neuwald, A.F., Aravind, L., Spouge, J.L. & Koonin, E.V. (1999) AAA+: A class of chaperone-like ATPases associated with the assembly, operation, and disassembly of protein complexes. Genome Research, 9, 27–43.

Olivares, A.O., Baker, T.A. & Sauer, R.T. (2016) Mechanistic insights into bacterial AAA+ proteases and protein-remodelling machines. Nature Reviews. Microbiology, 14, 33–44.

Piao, W., Kim, S.H., Lee, B.D., An, G., Sakuraba, Y. & Paek, N.C. (2019) Rice transcription factor OsMYB102 delays leaf senescence by down-regulating abscisic acid accumulation and signaling. Journal of Experimental Botany, 70, 2699–2715.

Qu, Y.C., Sakoda, K., Fukayama, H., Kondo, E., Suzuki, Y., Makino, A. et al. (2021) Overexpression of both Rubisco and Rubisco activase rescues rice photosynthesis and biomass under heat stress. Plant, Cell and Environment, 44, 2308–2320.

Sakuraba, Y., Kim, D. & Paek, N.C. (2018) Salt treatments and induction of senescence. Methods in Molecular Biology, 1744, 141–149.

Salekdeh, G.H., Siopongco, J., Wade, L.J., Ghareyazie, B. & Bennett, J. (2002) Proteomic analysis of rice leaves during drought stress and recovery. Proteomics, 2, 1131–1145.

Salvucci, M.E. (2008) Association of Rubisco activase with chaperonin-60beta: a possible mechanism for protecting photosynthesis during heat stress. Journal of Experimental Botany, 59, 1923–1933.

Salvucci, M.E., Portis, A.R. & Ogren, W.L. (1986) Light and $CO_2$ response of Ribulose-1,5-bisphosphate carboxylase/oxygenase activation in Arabidopsis leaves. Plant Physiology, 80, 655–659.

Salvucci, M.E., Werneke, J.M., Ogren, W.L. & Portis, A.R. (1987) Purification and species distribution of rubisco activase. Plant Physiology, 84, 930-936.

Sarwat, M., Naqvi, A.R., Ahmad, P., Ashraf, M. & Akram, N.A. (2013) Phytohormones and microRNAs as sensors and regulators of leaf senescence: assigning macro roles to small molecules. Biotechnology Advances, 31, 1153–1171.

Schippers, J.H., Schmidt, R., Wagstaff, C. & Jing, H.C. (2015) Living to die and dying to live: the survival strategy behind leaf senescence. Plant Physiology, 169, 914–930.

Schwab, R., Ossowski, S., Riester, M., Warthmann, N. & Weigel, D. (2006) Highly specific gene silencing by artificial microRNAs in Arabidopsis. Plant Cell, 18, 1121–1133.

Shen, J.B., Orozco, E.M., Jr. & Ogren, W.L. (1991) Expression of the two isoforms of spinach ribulose 1,5-bisphosphate carboxylase activase and

essentiality of the conserved lysine in the consensus nucleotide-binding domain. The Journal of Biological Chemistry, 266, 8963–8968.
Shim, K.C., Kim, S.H., Jeon, Y.A., Lee, H.S., Adeva, C., Kang, J.W. et al. (2020) A RING-type E3 ubiquitin ligase, OsGW2, controls chlorophyll content and dark-induced senescence in rice. International Journal of Molecular Sciences, 21, 1704.
Shim, Y., Kang, K., An, G. & Paek, N.C. (2019) Rice DNA-binding one zinc finger 24 (OsDOF24) delays leaf senescence in a Jasmonate-mediated pathway. Plant & Cell Physiology, 60, 2065–2076.
Song, Y., Yang, C., Gao, S., Zhang, W., Li, L. & Kuai, B. (2014) Age-triggered and dark-induced leaf senescence require the bHLH transcription factors PIF3, 4, and 5. Molecular Plant, 7, 1776–1787.
Suganami, M., Suzuki, Y., Kondo, E., Nishida, S., Konno, S. & Makino, A. (2020) Effects of overproduction of Rubisco activase on Rubisco content in transgenic rice grown at different N levels. International Journal of Molecular Sciences, 21, 1626.
Suganami, M., Suzuki, Y., Sato, T. & Makino, A. (2018) Relationship between Rubisco activase and Rubisco contents in transgenic rice plants with overproduced or decreased Rubisco content. Soil Science & Plant Nutrition, 64, 352–359.
Suganami, M., Suzuki, Y., Tazoe, Y., Yamori, W. & Makino, A. (2021) Co-overproducing Rubisco and Rubisco activase enhances photosynthesis in the optimal temperature range in rice. Plant Physiology, 185, 108–119.
Suzuki, G., Lucob-Agustin, N., Kashihara, K., Fujii, Y., Inukai, Y. & Gomi, K. (2021) Rice MEDIATOR25, OsMED25, is an essential subunit for jasmonate-mediated root development and OsMYC2-mediated leaf senescence. Plant Science, 306, 110853.
To, K.Y., Suen, D.F. & Chen, S.C. (1999) Molecular characterization of ribulose-1,5-bisphosphate carboxylase/oxygenase activase in rice leaves. Planta, 209, 66–76.
Uji, Y., Akimitsu, K. & Gomi, K. (2017) Identification of OsMYC2-regulated senescence-associated genes in rice. Planta, 245, 1241–1246.
van der Graaff, E., Schwacke, R., Schneider, A., Desimone, M., Flugge, U.I. & Kunze, R. (2006) Transcription analysis of Arabidopsis membrane transporters and hormone pathways during developmental and induced leaf senescence. Plant Physiology, 141, 776–792.
Waheeda, K., Kitchel, H., Wang, Q. & Chiu, P.L. (2023) Molecular mechanism of Rubisco activase: dynamic assembly and Rubisco remodeling. Frontiers in Molecular Biosciences, 10, 1125922.
Wang, D., Li, X.F., Zhou, Z.J., Feng, X.P., Yang, W.J. & Jiang, D.A. (2010) Two Rubisco activase isoforms may play different roles in photosynthetic heat acclimation in the rice plant. Physiologia Plantarum, 139, 55–67.
Wang, F., Cheng, Z., Wang, J., Zhang, F., Zhang, B., Luo, S. et al. (2022) Rice STOMATAL CYTOKINESIS DEFECTIVE2 regulates cell expansion by affecting vesicular trafficking in rice. Plant Physiology, 189, 567–584.
Wang, J., Qin, H., Zhou, S., Wei, P., Zhang, H., Zhou, Y. et al. (2020) The ubiquitin-binding protein OsDSK2a mediates seedling growth and salt responses by regulating gibberellin metabolism in rice. Plant Cell, 32, 414–428.
Werneke, J.M., Chatfield, J.M. & Ogren, W.L. (1989) Alternative mRNA splicing generates the two ribulosebisphosphate carboxylase/oxygenase activase polypeptides in spinach and Arabidopsis. Plant Cell, 1, 815–825.
Woo, H.R., Kim, H.J., Lim, P.O. & Nam, H.G. (2019) Leaf senescence: systems and dynamics aspects. Annual Review of Plant Biology, 70, 347–376.
Wu, Q., Han, T., Yang, L., Wang, Q., Zhao, Y., Jiang, D. et al. (2021) The essential roles of OsFtsH2 in developing the chloroplast of rice. BMC Plant Biology, 21, 445.
Wu, Z., Li, T., Zhang, Y., Zhang, D. & Teng, N. (2023) HD-Zip I protein LlHOX6 antagonizes homeobox protein LlHB16 to attenuate basal thermotolerance in lily. Plant Physiology, 194, 1870–1888.
Yang, Y., Yu, C.L., Wang, X.M., Yan, C.Q., Cheng, Y. & Chen, J.P. (2011) Inoculation with Xanthomonas oryzae pv. oryzae induces thylakoid membrane association of Rubisco activase in Oryza meyeriana. Journal of Plant Physiology, 168, 1701–1704.
Yi, L., Liu, B., Nixon, P.J., Yu, J. & Chen, F. (2022) Recent advances in understanding the structural and functional evolution of FtsH proteases. Frontiers in Plant Science, 13, 837528.
Yu, F., Park, S. & Rodermel, S.R. (2005) Functional redundancy of AtFtsH metalloproteases in thylakoid membrane complexes. Plant Physiology, 138, 1957–1966.
Zhang, J., Li, H., Xu, B., Li, J. & Huang, B. (2016) Exogenous melatonin suppresses dark-induced leaf senescence by activating the superoxide dismutase-catalase antioxidant pathway and down-regulating chlorophyll degradation in excised leaves of Perennial Ryegrass (Lolium perenne L.). Frontiers in Plant Science, 7, 1500.
Zhang, J. & Sun, A. (2009) Genome-wide comparative analysis of the metalloprotease ftsH gene families between Arabidopsis thaliana and rice. Chinese Journal of Biotechnology, 25, 1402–1408.
Zhang, N., Kallis, R.P., Ewy, R.G. & Portis, A.R., Jr. (2002) Light modulation of Rubisco in Arabidopsis requires a capacity for redox regulation of the larger Rubisco activase isoform. Proceedings of the National Academy of Sciences of the United States of America, 99, 3330–3334.
Zhang, N. & Portis, A.R., Jr. (1999) Mechanism of light regulation of Rubisco: a specific role for the larger Rubisco activase isoform involving reductive activation by thioredoxin-f. Proceedings of the National Academy of Sciences of the United States of America, 96, 9438–9443.
Zhang, Y., Dong, G., Wu, L., Wang, X., Chen, F., Xiong, E. et al. (2023) Formin protein DRT1 affects gross morphology and chloroplast relocation in rice. Plant Physiology, 191, 280–298.
Zhang, Y., Tan, S., Gao, Y., Kan, C., Wang, H.L., Yang, Q. et al. (2022) CLE42 delays leaf senescence by antagonizing ethylene pathway in Arabidopsis. The New Phytologist, 235, 550–562.
Zhang, Y.L., Dong, G.J., Wu, L.M., Chen, F., Yu, Y.C. & Ma, D.R. (2021) Identification and characterization of profilin gene family in rice. Electronic Journal of Biotechnology, 54, 47–59.
Zhang, Z. & Komatsu, S. (2000) Molecular cloning and characterization of cDNAs encoding two isoforms of ribulose-1,5-bisphosphate carboxylase/oxygenase activase in rice (Oryza sativa L.). Journal of Biochemistry, 128, 383–389.
Zhang, Z., Liu, H., Sun, C., Ma, Q., Bu, H., Chong, K. et al. (2018) A $C_2H_2$ zinc-finger protein OsZFP213 interacts with OsMAPK3 to enhance salt tolerance in rice. Journal of Plant Physiology, 229, 100–110.
Zhao, C., Wang, Y., Chan, K.X., Marchant, D.B., Franks, P.J., Randall, D. et al. (2019) Evolution of chloroplast retrograde signaling facilitates green plant adaptation to land. Proceedings of the National Academy of Sciences of the United States of America, 116, 5015–5020.